# Performance improvement of ballasted railway tracks using geocells

Nimbalkar, Sanjay; Punetha, Piyush; Kaewunruen, Sakdirat

# “Performance improvement of ballasted railway tracks using geocells: present status and future prospects” (Tentative)

Sanjay Nimbalkar[1[0000-0002-1538-3396]], Piyush Punetha[1[0000-0002-0812-4708]] and Sakdirat Kaewunruen[2[0000-0003-2153-3538]]

[1] University of Technology Sydney, NSW 2000, Australia
[2] The University of Birmingham, Edgbaston, B152TT UK
Email: Sanjay.Nimbalkar@uts.edu.au

**Abstract.** The dramatic increase in the axle load and speed of the rolling stock over the recent years has challenged the stability and performance of the railway tracks. Consequently, rail track designers and engineers are exploring suitable measures to improve the performance of the tracks. The geocells can offer a cost-effective and feasible solution for enhancing the performance of the railway tracks. The satisfactory performance of geocells in numerous geotechnical applications such as reinforced retaining walls, slopes, embankments, pavements, etc. have encouraged their use in other areas too. However, their utilization in the railway tracks is still in the nascent stage. Thus, the present chapter examines the potential benefits of using geocells in the railway tracks. The results of the numerous experimental, numerical and field studies have been briefly reviewed. The influence of geocell reinforcement on the parameters (or material properties) essential for the track stability have been discussed. The past studies indicate that the geocells can be effectively used to improve the performance of the railway tracks. The geocells provides confinement which increases the strength and stiffness of the infill materials. Moreover, the geocell reinforcement significantly decreases the lateral deformation and permanent settlement of the granular materials. However, the amount of improvement significantly depends on the properties of the geocell, infill, subgrade and the location of the geocell reinforced layer.

**Keywords:** Geocell, Railways, Resilient modulus, Permanent deformation, Confinement, Analytical model.

## 1 Introduction

The rapid growth in population has substantially increased the passenger and goods traffic throughout the world [1]. Therefore, the demand on the transportation facilities is escalating tremendously [2]. To cater to such huge demands, the existing modes of transportation are undergoing a rapid expansion in their infrastructure [3]. Consequently, the number of road vehicles and aircraft has significantly increased. Howev-

er, the increase in the number of vehicles has resulted in a tremendous amount of congestion and air pollution [4-6].

The rail transport, on the other hand, is considered as an environment-friendly mode of transportation for carrying a large volume of freight and passengers over long distances [6]. Similar to its counterparts, the rail transport has tackled the hike in demand by increasing the speed of passenger vehicles and by increasing the capacity of the freight trains [2]. Consequently, the frequency and magnitude of the load on the existing railway tracks have dramatically increased [7]. However, most of the existing tracks have not been designed for such intensity and frequency of loads. Therefore, the stability of the track may get compromised in most of the conventional tracks [3].

The stability of a railway track is inevitable for the smooth and safe operation of the railway traffic, whether it be a passenger train, a freight train or other rolling stock. The track deterioration poses severe consequences on the safety of the trains [8]. Moreover, the track instability reduces the comfort of the passengers and may even endanger their lives.

The stability of a railway track depends on the hydraulic and mechanical behavior of the constituent materials (such as ballast, sub-ballast, etc.) and the soil subgrade under the train-induced quasi-static and dynamic loading. Throughout the service life, the track is subjected to repetitive loads due to the movement of the trains. With an increase in the frequency and magnitude of the load, the subgrade and the constituent materials undergo a tremendous amount of deformation and deterioration [9]. This degradation leads to unacceptable differential settlements, lateral instability and a loss of track geometry [10]. Consequently, the track loses its efficiency and demands for either restriction in the maximum train speed or costly maintenance and upgrade [9].

The maintenance work usually involves the replacement of the deteriorated constituent materials. However, the disposal of a massive quantity of the degraded material poses a serious challenge to the rail authorities due to the strict regulations established by the environment protection agency [11]. An alternative is to recycle the degraded material and re-use it for the construction of the tracks. Additionally, the locally available materials could also be used to reduce the overall maintenance costs [4]. However, the recycled and locally available materials often possess inadequate strength and stiffness for the application in the railway tracks. Therefore, the use of these inferior quality materials may be detrimental for the track performance and may lead to extensive lateral spreading and differential settlements.

The geosynthetics can offer an economical and feasible solution for improving the performance of the railway tracks [4, 12-15]. Geosynthetics are the polymeric materials that are used for numerous applications such as soil reinforcement, slope stabilization, filtration, drainage, etc. [16]. They have become an indispensable component in most of the geotechnical engineering projects. Moreover, the geosynthetics such as geogrids, geotextiles, and geocomposites have been used successfully for a long period in the railways for improving the stability of the tracks on soft subgrade [17].

The railway tracks often undergo a significant amount of lateral spreading owing to insufficient confinement, especially when the subgrade is stiff [4]. The geosynthetics, such as geocell can reduce this lateral deformation by confining the constituent materials. Geocell is a three-dimensional honey-comb shaped polymeric material that is

used to improve the strength and stiffness of the granular materials by providing additional confinement [18]. The geocells have been used for the construction of slopes, embankments, retaining walls, pavements, etc., however, their utilization in the field of railways is still minimal (e.g., [19, 20]. The limited application in the railways is probably due to the lack of available design guidelines or due to the conservative approach of the railroad track designers [21]. Several studies on the beneficial role of geocell have been carried out (e.g. [4, 18, 21-29]. However, most of the studies primarily focus on the pavements and only a few of them discuss the performance of geocells in the actual railway tracks.

The present chapter aims to explore the beneficial role of geocell in enhancing the stability of the railway tracks. The chapter is presented in the following sequence: first, the basic concepts for track design are briefly discussed. Subsequently, the potential benefits of using geocell in railways such as improvement in resilient modulus, reduction in plastic deformation, additional confinement, etc. and the mathematical models that can be used for their quantification are described. Finally, the factors affecting the application of geocells in the railway tracks are discussed.

## 2 Railway track - basic concepts

The railway track is the structure on which the trains and other rolling stock move. The primary function of a railway track is to provide a stable and robust bed for the movement of the trains. Moreover, the track must be able to transfer the traffic induced loads safely to the soil. Safety implies that the stresses transferred to the soil must be within the permissible limits, enabling a sufficient safety margin for various risks and uncertainties [30].

### 2.1 Structure of the ballasted railway track

The ballasted railway tracks employ multiple layers of unbound granular material (ballast and sub-ballast) to transfer the train-induced loads safely to the subgrade. These tracks consist of two essential components: superstructure and substructure. The superstructure comprises of rails, rail pads, sleepers (or ties) and the fasteners. Moreover, the substructure constitutes of the ballast, sub-ballast and soil subgrade (or formation). Fig. 1 shows a typical cross-section of the ballasted track above the soil subgrade.

The rail is a longitudinal steel member which is supported by sleepers at regular intervals. It provides a firm base for the movement of trains. It must possess adequate strength and stiffness to resist the forces exerted by the rolling stock without undergoing significant deformation. The rail primarily accommodates the wheel and transfers the load from the train to the sleepers. Moreover, it may also serve as an electric signal conductor in an electrified line [7, 31].

The fasteners are used to maintain the position of the rail on the sleepers. They resist a combination of train-induced vertical, lateral and longitudinal forces in addition to the overturning moments [31].

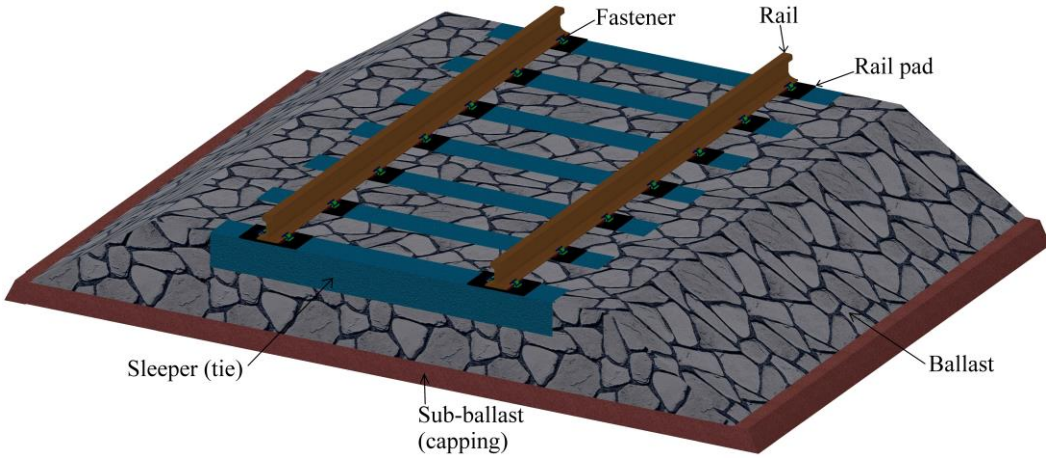


**Fig. 1.** Ballasted track structure

The rail pads are often provided below the rail to filter out or dampen the dynamic forces generated from the movement of the high speed rolling stock [7]. Therefore, they reduce the amount of vibration transmitted to the sleeper and the substructure.

The sleepers (or ties) are the transverse beams that support the rails and transfer the traffic induced vertical, lateral and longitudinal forces to the substructure [32]. The sleepers can be manufactured using steel, concrete or timber. However, the pre-stressed concrete sleepers are the most commonly used sleepers due to their high strength and durability [31].

The ballast bed is a layer of coarse-aggregates that provides support to the sleepers. It comprises of crushed stones and gravel with a typical particle size range between 20-60 mm [30]. The primary functions of the ballast bed are to provide a stiff bearing surface for the sleepers and to transfer the imposed superstructure loads safely to the sub-ballast and the subgrade [32]. Moreover, the ballast bed facilitates the drainage of water away from the track, reduces vibrations and absorbs the noise [8].

The sub-ballast bed (capping) is a layer of granular material that acts as a filter to prevent the movement of fines from the subgrade to the ballast. Moreover, it arrests the penetration of the ballast into the subgrade and drains water away from the sub-grade into the ditches. The sub-ballast layer also distributes the traffic induced stress-es uniformly over a wide area of the subgrade [7].

The subgrade is the lowermost part of the railway track that ultimately bears the weight of the track and the traffic induced loads. The safety and long-term perfor-mance of a track primarily depend on the mechanical and hydraulic behavior of the subgrade. Therefore, it must possess adequate strength (bearing capacity), stiffness and drainage ability.

## 2.2 Loads on a track

A railway track withstands a combination of loads in vertical, lateral and longitudinal directions resulting from the traffic, track condition and temperature. The vertical load is primarily due to the weight of the rolling stock. In addition to the weight, the vertical forces also emerge due to the movement of the vehicle on the track with geometrical irregularities. These forces are known as the dynamic forces, and their magnitude and frequency depend on the amount of rail/vehicle irregularities [31]. The lateral loading arises from the wind, train's reaction to geometric deviations in the track, centrifugal force in curves, buckling reaction force on the rail (at high rail temperatures), etc. [7]. Moreover, the longitudinal loading originates from the traction and braking forces from the trains, thermal effects and wave action of rail [8].

**Vertical load.**

The vertical load is a complex combination of moving static and dynamic loads [30]. The total vertical load on a railway track is given as (Eq. 1):

$$P_{total} = P_{quasi-static} + P_{dynamic} \tag{1}$$

where, $P_{total}$ is the total vertical wheel load; $P_{quasi\text{-}static}$ is the quasi-static wheel load, which is the sum of the static wheel load, wind load and non-compensated centrifugal force on the outer rail (in a curve); $P_{dynamic}$ is the dynamic component of load that depends on the speed of the train, quality of the track and the wheel, vehicle parameters (such as wheel diameter and unsprung mass), etc.

$$P_{quasi-static} = \left(\frac{P}{2}\right) + H_w \frac{l_w}{b_t} + P \frac{l_c}{{b_t}^2}\left(\frac{b_t V^2}{g R_c} - h_s\right) \tag{2}$$

where, $P$ is the static axle load; $H_w$ is the crosswind force; $l_w$ is the distance between center of rail and the resultant wind force; $l_c$ is the distance between centroid of rail and center of gravity of the train; $b_t$ is the track width; $V$ is the train speed; $g$ is the acceleration due to gravity; $R_c$ is the radius of curvature of track; $h_s$ is the super-elevation.

The dynamic component of the load is very complex as it depends on a large number of parameters such as track geometry, train configuration and speed, etc. Consequently, the dynamic effect is represented in the form of a factor which is multiplied to the static wheel load (Eq. 3) [31, 32]. This factor is known as the dynamic amplification factor (DAF) or the impact factor, and it depends on the parameters such as the train speed, quality (or condition) of the rail and wheel, the stiffness of subgrade, etc. [33].

$$P_d = \varphi P_0 \tag{3}$$

where, $P_d$ is the design wheel load (kN); $\varphi$ is the DAF (always greater than 1); $P_0$ is the static wheel load (kN). Table 1 shows the different empirical equations to evaluate the DAF. The details of the methods can be found elsewhere [7, 32, 34].

**Table 1.** Empirical equations to calculate the impact factor of DAF

| Method | Equation | Remarks |
|---|---|---|
| AREA [35] | $\varphi = 1 + \frac{0.00521 \cdot V}{D_w}$ | $V$ is the speed of the train (km/h); $D_w$ is the diameter of wheel (m). |
| Eisenmann [36] | $\varphi = 1 + \delta\eta t$<br>$\eta = 1$, for $V$< 60 km/h<br>$\eta = \left(1 + \frac{V-60}{140}\right)$, for $60 \leq V \leq 200$ km/h | $\delta$ is a factor that depends on the track condition; $\eta$ is a factor that depends on the speed of the vehicle; $t$ is a factor that depends on the upper confidence limit. |
| ORE [32, 37] | $\varphi = 1 + \alpha' + \beta' + \gamma'$<br>$\alpha' = 0.04\left(\frac{V}{100}\right)^3$<br>$\beta' = \frac{V^2(2h+h_s)}{127 R_c l_g} - \frac{2h_s h}{l_g^2}$<br>$\gamma' = 0.1 + 0.017\left(\frac{V}{100}\right)^3$ | $\alpha'$ is a coefficient that depends on the track irregularities, train suspension, and speed; $\beta'$ is a coefficient that accounts for the movement of train along a curve, $\gamma'$ is a coefficient that depends on the train speed and configuration, and track condition; $V$ is the speed of train (km/h), $h_d$ is the cant/super-elevation deficiency (m), $l_h$ is the gauge width (m), $h$ is the vertical distance from rail top to center of mass of train (in m), $h_s$ is the super-elevation (m), $R_c$ is the radius of curvature (m). |
| Atalar et al. [38] | $\varphi = \left(1 + \frac{V}{100}\right)(1 + C)$ | $C$ is a coefficient (value ≈ 0.3); $V$ is the speed of the train (km/h). |
| British Railways [32] | $\varphi = 1 + \frac{8.784(\theta_1+\theta_2)V}{P_0}\left(\frac{K_j W_u}{g}\right)^{0.5}$ | $(\theta_1 + \theta_2)$ is the total dip angle of the rail joint (radians); $V$ is the train speed (km/h); $P_0$ is the static wheel load (kN); $K_j$ is the track stiffness at joint (kN/mm); $W_u$ is the unsprung weight at one wheel (kN); $g$ is the acceleration due to gravity (m/s$^2$). |
| Indian Railways [32] | $\varphi = 1 + \frac{V}{58.14(k)^{0.5}}$ | $V$ is the speed of the train (km/h); $k$ is the track modulus (MPa) |
| German formula [32] | $\varphi = 1 + \frac{V^2}{3\times10^4}$ (for $V \leq 100$ km/h)<br>$\varphi = 1 + \frac{4.5\,V^2}{10^5} - \frac{1.5\,V^3}{10^7}$ (for $V$>100 km/h) | $V$ is the speed of train (km/h) |
| South African formula [32] | $\varphi = 1 + \frac{4.92 \cdot V}{D_w}$ | $D_w$ is the diameter of wheel (mm) |
| WMATA [34] | $\varphi = (1 + 0.0001V^2)^{0.67}$ | $V$ is the speed of train (miles/h) |

**Lateral loads.**

The loads acting on the railhead in the lateral direction depend on the parameters such as the radius of curvature of the track, speed and configuration of the train, etc. [32]. Several empirical expressions have been developed (based on the field investigations) to evaluate the magnitude of the lateral load exerted by the wheel flange on the railhead while negotiating the curves. Some of the empirical expressions are discussed here [32].

*ORE formula.*

The ORE conducted field investigations to evaluate the magnitude of the lateral load exerted by the wheel flange on the railhead for different train configurations, speed (up to 200 km/h) and curve radii. The results showed that the lateral force depends only on the radius of curvature of the track. Moreover, the following equation (Eq. 4) was developed to calculate the magnitude of the lateral load:

$$H = 35 + \frac{7400}{R_c} \tag{4}$$

where, $H$ is the lateral load (kN); $R_c$ is the radius of curvature of the track.

*Swedish Railways formula.*

The Swedish Railways conducted similar field investigations to evaluate the magnitude of the lateral load exerted by the wheel flange on the railhead for different train configurations, speed and a curve radius of 600 m. The following empirical expression was developed (Eq. 5):

$$H_{mean} = 17 + \frac{V}{27.6} \tag{5}$$

where, $H_{mean}$ is the mean lateral load (kN); $V$ is the speed of train (km/h).

*British Railways*

The British Railways recommend the use of following equation (Eq. 6) to evaluate the lateral load [39].

$$H = PA_d + A_y V_m \sqrt{\frac{M_u}{M_u + M_y}} \left(K_y M_u\right)^{0.5} \tag{6}$$

where, $A_d$ is the maximum normal operating cant deficiency angle; $V_m$ is maximum normal operating speed; $M_u$ is the effective lateral unsprung mass per axle; $A_y$ is the angle of lateral ramp discontinuity (0.0039 rad); $M_y$ is the effective lateral rail mass per wheel (170 kg); $K_y$ is the effective lateral rail stiffness per wheel ($25 \times 10^6$ N/m). As per the British standards [39], the total lateral load per axle on the track must not exceed 71 kN when a rolling stock negotiates a curve with a lateral ramp discontinuity at maximum permissible speed and cant deficiency. The maximum permissible value of 71 kN corresponds to the lateral force theoretically induced by a Class 86/2 electric locomotive travelling at a speed of 180 km/h over a curve with a lateral ramp in outer rail and a cant deficiency of 5.8° [40]. Moreover, the lateral load on the track per axle (sustained over a length ≥ 2 m) must never be greater than (P/3+10) kN.

**Longitudinal loads.**

The longitudinal loads develop from the thermal expansion and contraction of the rails, wheel action, and the traction and braking forces from the wheel. The thermal effects can lead to the buckling of the rail and are much more pronounced in the continuously welded rails. Moreover, the traction and braking result in excessive wear and tear in both rails and wheel [34].

**Impact loads.**

In addition to the quasi-static forces, the railway track is often subjected to impact loads due to inevitable track and vehicle abnormalities. The impact loads are characterized by a high magnitude and short duration. Worn wheel/rail surface profile, wheel flats, bad welds, switches, dipped rails, joints, rail corrugation, turnouts, unsupported sleepers, an abrupt change in track stiffness are some of the inevitable causative factors of the impact loads in a railway track [9, 31].

The impact loads generate two distinct force peaks. The first peak is characterized by a large magnitude and small duration (known as $P_1$). Whereas, the second peak is characterized by a small magnitude and large duration (known as $P_2$) [7]. The peak $P_1$ occurs due to the inertia of the rail and sleepers and it doesn't affect the track substructure. However, the peak $P_2$ occurs due to the mechanical resistance offered by the track substructure [7] and is responsible for the deterioration of the constituent materials of the track [41].

The $P_2$ force can be evaluated using the following formula [42] (Eq. 7):

$$P_2 = Q + (A_z V_m M C' K) \tag{7}$$

where, $Q$ is the maximum static wheel load (N); $V_m$ is the maximum normal operating speed of train (m/s); $A_z$ is total angle of vertical ramp discontinuity (0.02 rad).

$$M = \left(\frac{M_v}{M_v + M_z}\right)^{0.5} \tag{8}$$

$$C' = 1 - \left(\frac{\pi C_z}{4\{K_z(M_v + M_z)\}^{0.5}}\right) \tag{9}$$

$$K = (\mathrm{K}_z M_v)^{0.5} \tag{10}$$

where, $M_v$ is effective vertical unsprung mass per wheel (kg); $M_z$ is effective vertical rail mass per wheel (245 kg); $C_z$ is effective vertical rail damping rate per wheel ($55.4 \times 10^3$ Ns/m); $K_z$ is the effective vertical rail stiffness per wheel ($62 \times 10^6$ N/m).

The British standards restrict the maximum value of $P_2$ force to 322 kN per wheel [39]. The maximum permissible value of 322 kN corresponds to the $P_2$ force theoretically induced by the Class 55 Deltic locomotive while travelling over a dipped rail joint (total dip angle of 0.02 rad) with a speed of 161 km/h [40].

The impact loads induce vibrations and oscillations in the train body and the different track components. Additionally, they generate a considerable amount of noise that may be annoying to the nearby residents. The vibrations affect the performance of the track as well as the passenger comfort. The magnitude and nature of the vibra-

tion depend on the characteristics of the geometric irregularity of the track and the wheel. A geometric irregularity with a large wavelength (e.g., due to differential settlement of the track) primarily causes train body vibrations that reduce the comfort of the passengers. However, the irregularity with a small wavelength (wheel or rail corrugations) primarily generates the wheel vibration. The wheel vibration leads to the fluctuation in axle weight and results in the vibration in the track [43]. Moreover, the vibrations produced due to the impact loads accelerate the deterioration of the ballast and sub-ballast bed (especially for stiff subgrade) and consequently, endanger the stability and efficiency of a track [9]. The impact loads may also lead to the differential track settlement due to the localized compaction of the subgrade at the impact location [44].

### 2.3 Track design

The design of a ballasted railway track involves the determination of the stresses and settlements at critical locations within the track such as the sleeper-ballast, ballast-sub-ballast, and sub-ballast-subgrade interface. Subsequently, the magnitude of the induced stresses and settlements are compared with the permissible values to arrive at a suitable factor of safety [32]. The dimensions of the sleepers, and the thickness of the ballast and sub-ballast layers are then adjusted to control the magnitude of the stresses and settlements [32, 45]. Fig. 2 shows the flowchart for the design of a ballasted railway track.

The design technique uses semi-empirical equations to evaluate the load and deformations in the track. This is primarily due to the complexity in the accurate prediction of the train-induced loads and the corresponding track response. The loads are complex combinations of moving static and dynamic components (as discussed in the previous sections). Moreover, the track structure increases this complexity manifolds since it comprises different layers with distinct properties. Consequently, the present track design techniques are still very conservative and require further development [12].

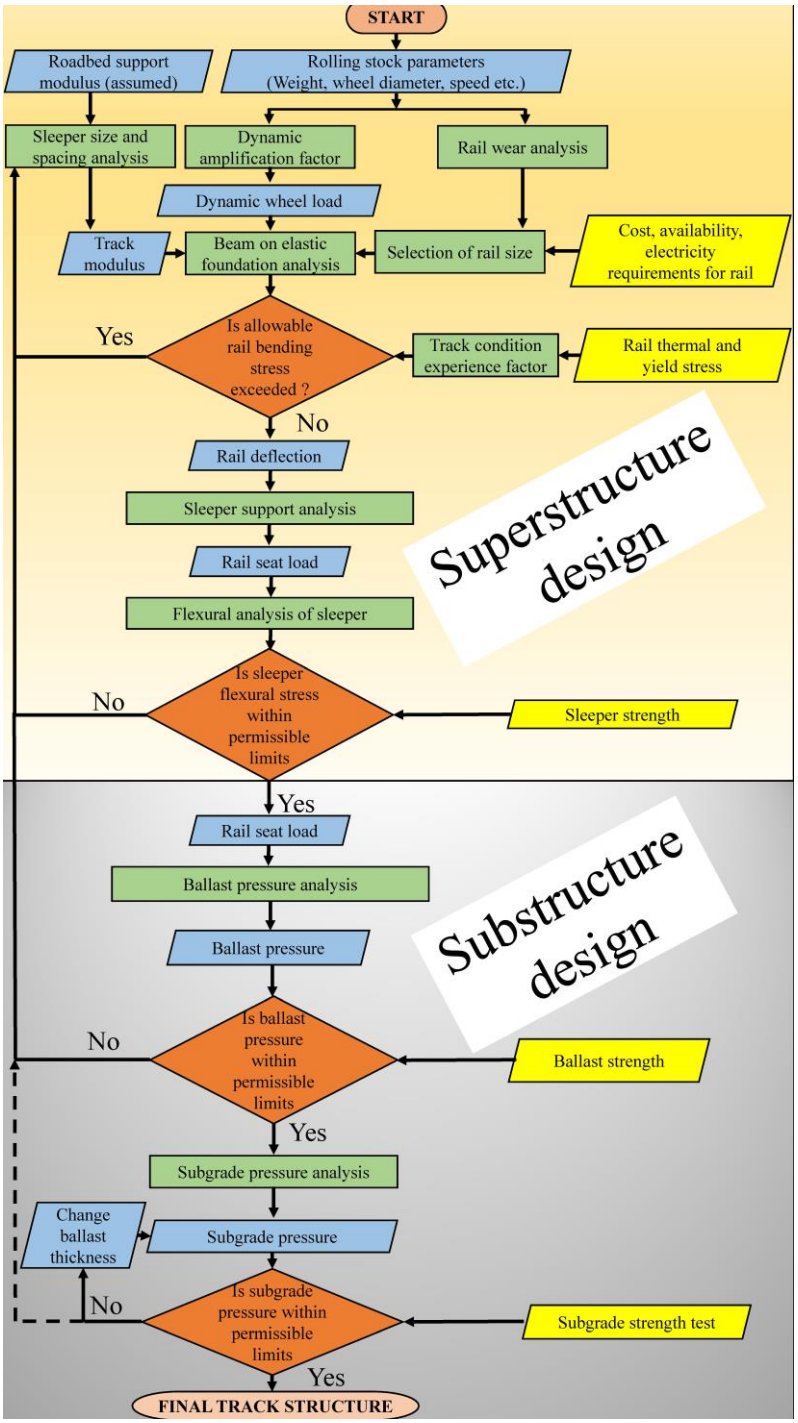


**Fig. 2.** Flowchart for the design of conventional ballasted track (modified from [32])

# 3 Beneficial role of geocell in railways

## 3.1 General.

The conventional ballasted tracks require frequent maintenance due to the deterioration/degradation of the constituent granular materials (e.g., ballast) under repeated traffic loading [30]. The degradation primarily involves the crushing or churning up of the ballast particles which produces fines. The fines clog the voids and decrease the permeability of the ballast bed. Additionally, the problems may arise due to mud pumping or the intrusion of clay and silt size particles from the subgrade (saturated, soft subgrade) into the ballast bed, lateral buckling of rails due to insufficient confinement, etc. [7].

The maintenance work is not only expensive but also disrupts the traffic and reduces the availability and efficiency of the track. Therefore, the rail-track designers are exploring suitable measures to improve the performance of the tracks and reduce the frequency of maintenance cycles. The geocells can provide a cost-effective solution in this aspect.

The use of geocell can be highly beneficial for the long-term stability of the railway tracks. Fig. 3 illustrates the need for using geocell in ballasted railway tracks. As discussed above, the traffic-induced load leads to the degradation of the constituent materials. Consequently, the track loses its geometry and efficiency and demands costly maintenance. The geocells provide confinement to the infill materials and may protect the track geometry for a long period which may reduce the frequency of maintenance cycles.

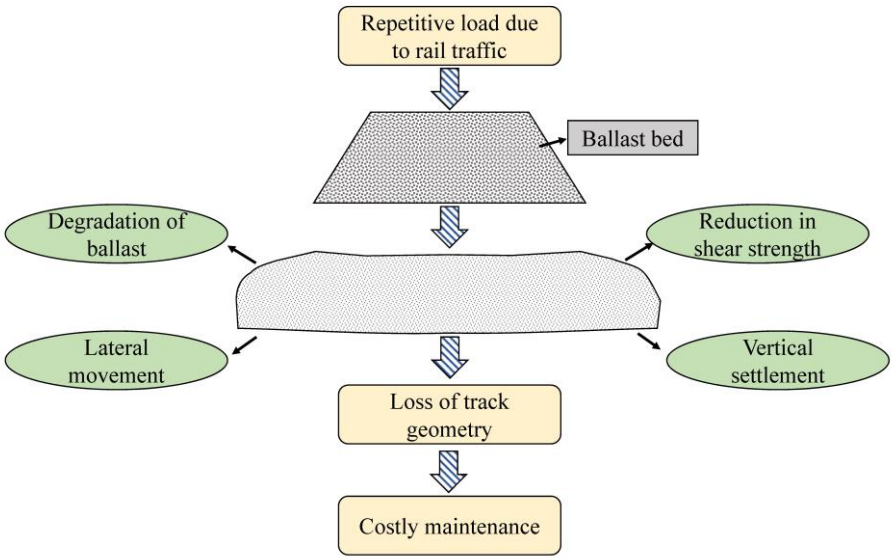


**Fig. 3.** Need for using geocell in ballasted railway tracks

Numerous experimental, numerical and analytical studies have indicated that the geocells can be used to improve the performance of a ballasted track [21, 29]. The results of the studies show that:

1. The geocell confines the infill material, which increases its strength and stiffness. Consequently, the traffic-induced stress gets uniformly distributed to a wider area [46, 47].
2. The geocell confinement reduces (redistributes) the shear stresses at the ballast (or sub-ballast)-subgrade interface [27].
3. The use of geocell preserves the track geometry by reducing the strain and permanent deformation in the subgrade. Moreover, it increases the strength and resilience of the infill material under cyclic loading [12, 19, 46].
4. The confinement provided by the geocell reduces the lateral deformations in the track and thus, maintains the track shape [18].

The amount of improvement in track stability depends on the location of the geocell reinforced layer. Several researchers have studied the performance of geocell reinforced infill layer at different locations within a track such as in the ballast bed, the sub-ballast or in the soil subgrade [4, 18, 29]. The ideal location of using geocell is in the ballast bed immediately below the sleepers. However, a minimum gap of 15–25 cm has to be maintained below the sleeper for the regular maintenance operations [18, 21]. Furthermore, the service life of the geocell may reduce when it is placed near the top of the ballast bed due to a large amount of bending [48].

The presence of geocell reinforced layer in the track substructure reduces the vertical stress which minimizes settlement and lateral spreading of the bottom layer [48]. The effectiveness of using geocell in reducing the settlement may decrease with an increase in depth of the geocell layer from the top (or base of sleepers). Fig. 4 shows the variation of subgrade stress below a railway track with (a) unreinforced ballast bed; (b) ballast bed reinforced with geocell near the sleeper base; (c) ballast bed reinforced with geocell at the bottom. It is apparent that the load is distributed uniformly over a wide area of the subgrade for geocell reinforced ballast. Moreover, the load spread area is higher when the geocell is placed near the sleeper as compared to the case when it is situated near the sub-ballast. This is because the geocell reinforced ballast is subjected to a high magnitude of vertical stress when it is placed near the top. Consequently, more confinement is mobilized and the load is spread over a wider area.

However, the geocell reinforced layer is subjected to low vertical stress when it is positioned near the base. Therefore, less confinement is mobilized and the load is distributed over a small area. Nevertheless, the amount of load spread also depends on the relative stiffness between the subgrade and the geocell reinforced layer [21]. The stiffness ratio between the geocell reinforced layer and subgrade must be large. However, there is an upper limit to the stiffness ratio because Leshchinsky and Ling [21] observed a non-uniform stress distribution at the subgrade due to the use of rigid (steel) geocell.

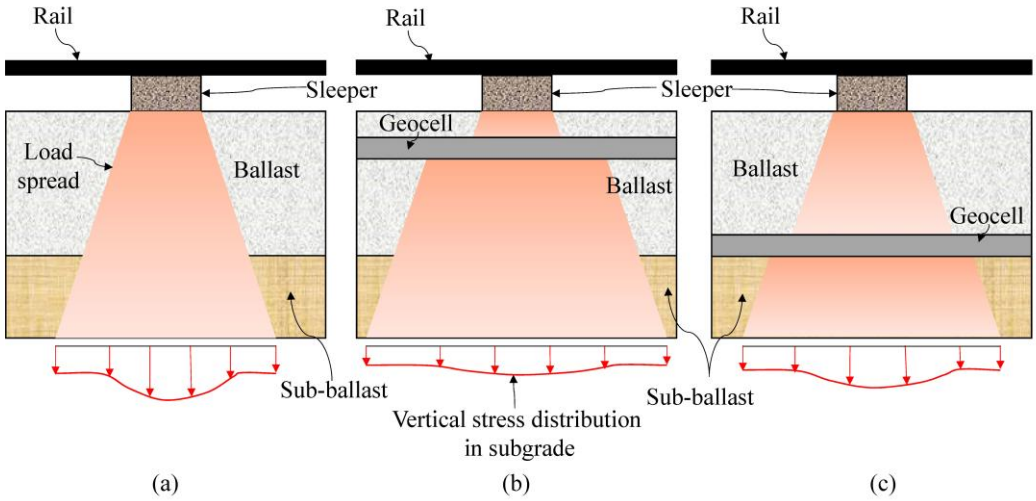


**Fig. 4.** The vertical stress distribution in the subgrade for the ballasted track (a) without geocell layer; (b) geocell layer near the top of ballast bed; (c) geocell layer near the bottom of ballast bed.

### 3.2 Case studies.

This section discusses a few case studies related to the beneficial role of geocells in the railway tracks.

**Reconstruction of ballasted track for gantry crane using geocells.**

Raymond [19] reported the reconstruction of a ballasted track for a gantry crane in Canada. A 200 mm thick geocell reinforced sub-ballast layer was provided below the sleepers (with a gap of 200 mm between sleeper and geocell layer) during the reconstruction. The use of geocell reduced the settlement and lateral deformation of the track significantly.

**Retrofitting of a portion of Amtrak's north-east corridor railway line using geocells.**

Zarembski et al. [20] discussed the reconstruction of a portion of Amtrak's north-east corridor railway line using geocell. The presence of soft subgrade in the site and extensive ballast fouling resulted in significant loss in track geometry which demanded frequent maintenance. Consequently, a layer of geocell was provided in the sub-ballast to reduce the subgrade stress and the track geometry degradation. Furthermore, a part of the track was reconstructed without geocell to compare the results. The field investigations revealed that the geocell stabilized section showed minimal amount of settlement and subgrade stress as compared to the non-reinforced section. Moreover, the rate of track geometry degradation reduced for the geocell reinforced track.

**Construction of a transition zone near a railway bridge in the south coast of New South Wales, Australia**.

Generally, the stiffness of a rail track is much higher at the bridge as compared to the bridge approaches. Therefore, train experiences an abrupt change in the track stiffness as it approaches the bridge. Consequently, the impact loads are generated at the wheel-rail interface which endangers the track stability. A transition zone is usually provided near the bridge end to gradually increase the track stiffness and prevent the generation of the impact loads. The geocells can be employed in the transition zones to increase the stiffness of the track and mitigate the impact loads.

Kaewunruen et al. [49] investigated the performance of a transition zone near a railway bridge on the south coast of New South Wales, Australia. The transition zone comprised of ALT1 baseplates, FLAT1 sleepers, and geocells to mitigate the traffic induced vibrations and increase the stiffness of the track. Fig. 5 shows the placement of the geocells in the transition zone.

**Fig. 5.** Installation of geocells at the railway bridge ends on the south coast line of New South Wales, Australia [49]

Additionally, SA-47 pads were provided with the sleepers immediately after the transition zone. Accelerometers were used to monitor the vibrations generated in the rail, sleepers and the ballast at the bridge, bridge ends, the transition zone, the section with SA-47 padded sleepers and the region with ordinary sleepers. Fig. 6 shows the location of the accelerometers along the tracks.

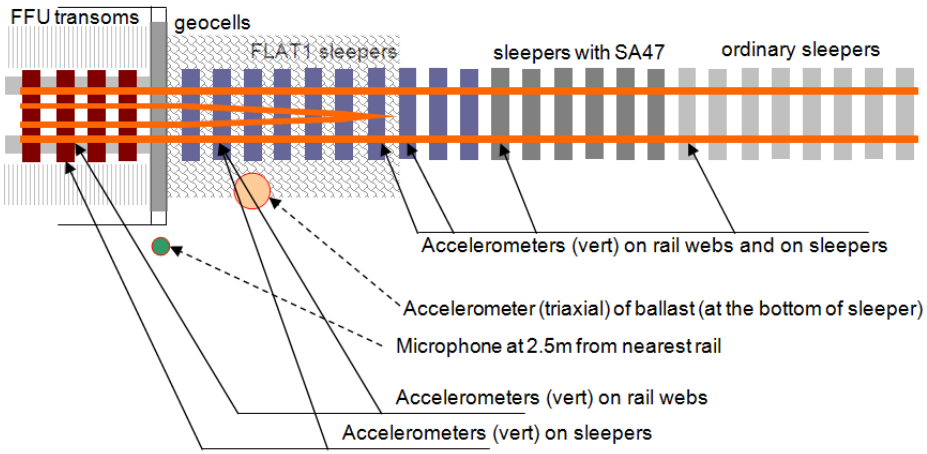


**Fig. 6.** Location of the accelerometers along the railway track [49]

Figs. 7-9 show the typical Fourier amplitude spectra of the acceleration recorded in different components of a railway track at different sections (for passage of three different trains) [49]. It is apparent from the figures that as the trains move from the region with ordinary sleepers towards the bridge, the vibration in the sleepers increases. However, the magnitude of vibration is almost identical at the bridge end and the transition zone. This behavior may be attributed to the increased stiffness of the track by the use of geocells in the transition zone which mitigated the impact loads on the track. Moreover, Fig. 9 shows that the magnitude of vibration in the ballast is very small as compared to the sleepers.

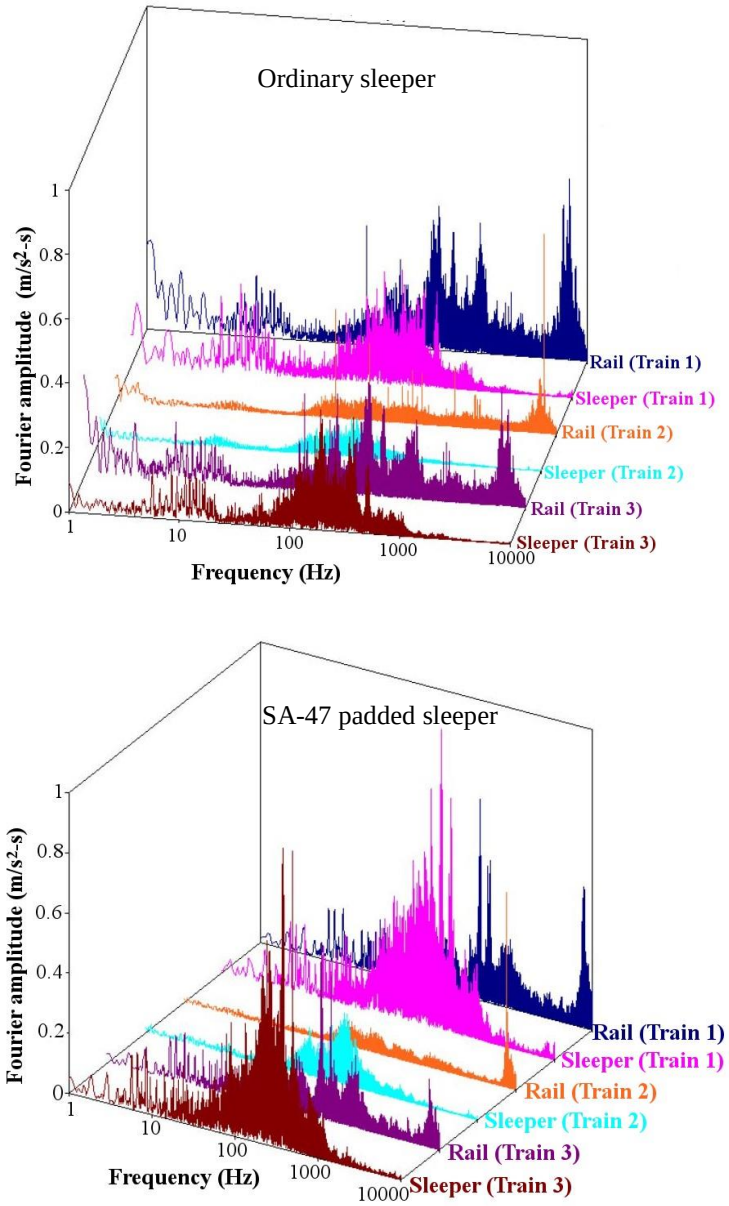


**Fig. 7.** Typical Fourier amplitude spectrum for field accelerometer data recorded at the region with ordinary sleeper and the section with SA-47 padded sleeper [49]

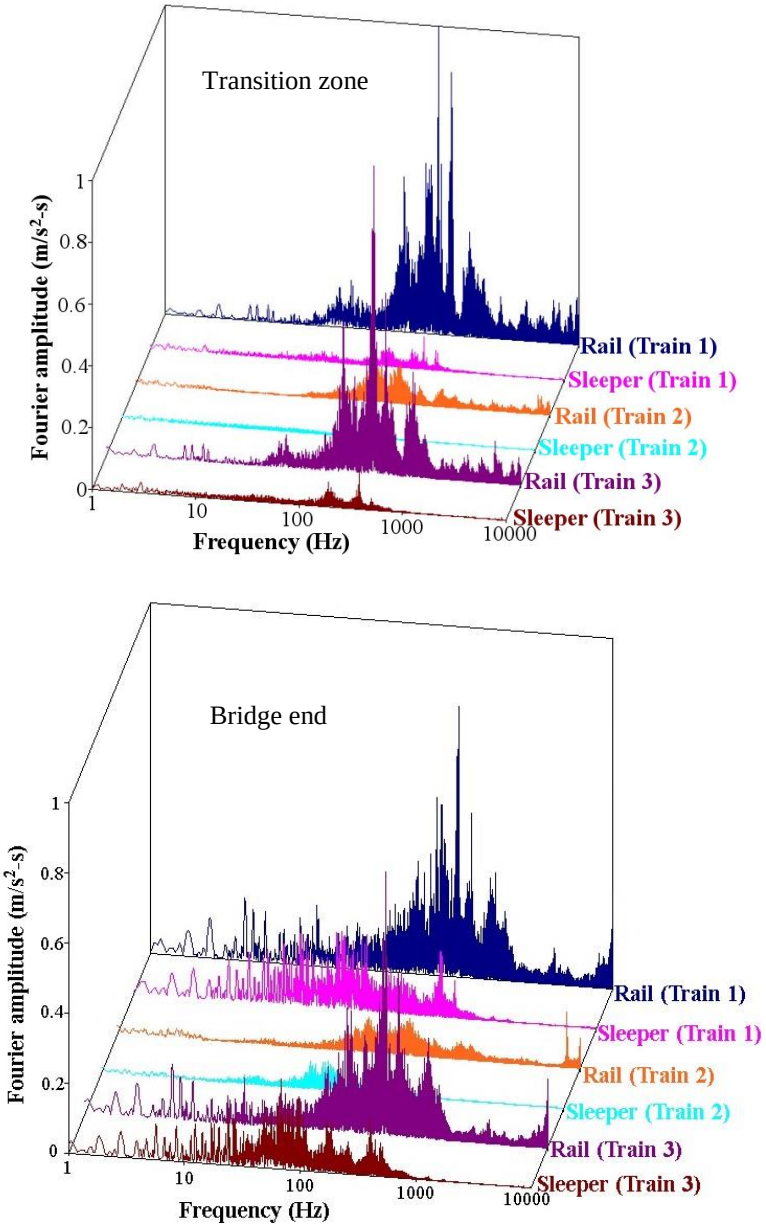


**Fig. 8.** Fourier amplitude spectrum for field accelerometer data recorded in the transition zone and at the bridge end [49]

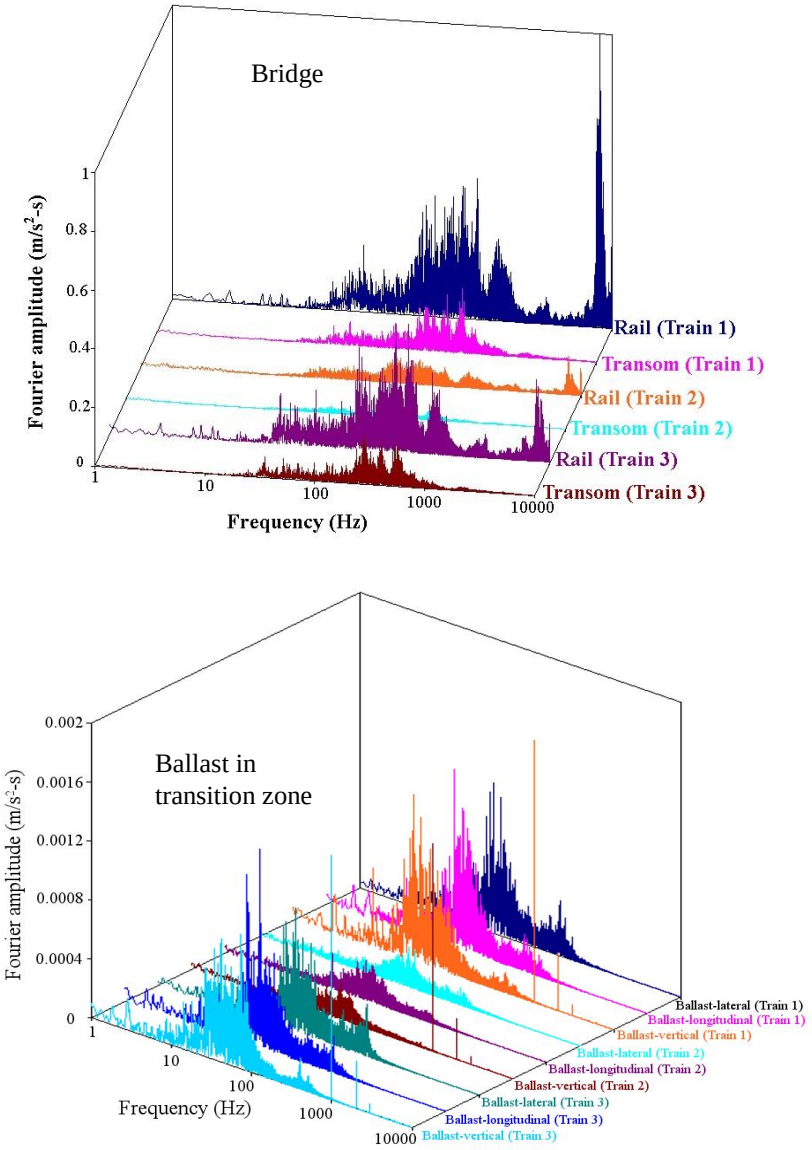


**Fig. 9.** Fourier amplitude spectrum for field accelerometer data recorded at the bridge and the ballast in transition zone [49].

Fig. 10 shows the deviations in track geometry after the construction of the transition zone. The data has been obtained from the axle-box accelerometers installed in an inspection vehicle. The transition zone was constructed in late November 2012. The figure shows the track geometry measurements taken immediately after the construction i.e. in December 2012 and after 7 months of construction i.e. in July, 2013.

The track was bi-directional, therefore, the data was taken in both up and down directions. The up and down directions correspond to the cases when the bridge end act as the exit end and the entrance end, respectively.

The figure shows that the deviation in the track is almost identical for both the measurements conducted in December 2012 and July 2013. This observation clearly indicates that the rate of track geometry deterioration is very slow. This slow rate of deterioration is probably due to the mitigation of impact forces by the installation of geocell layer in the transition zone.

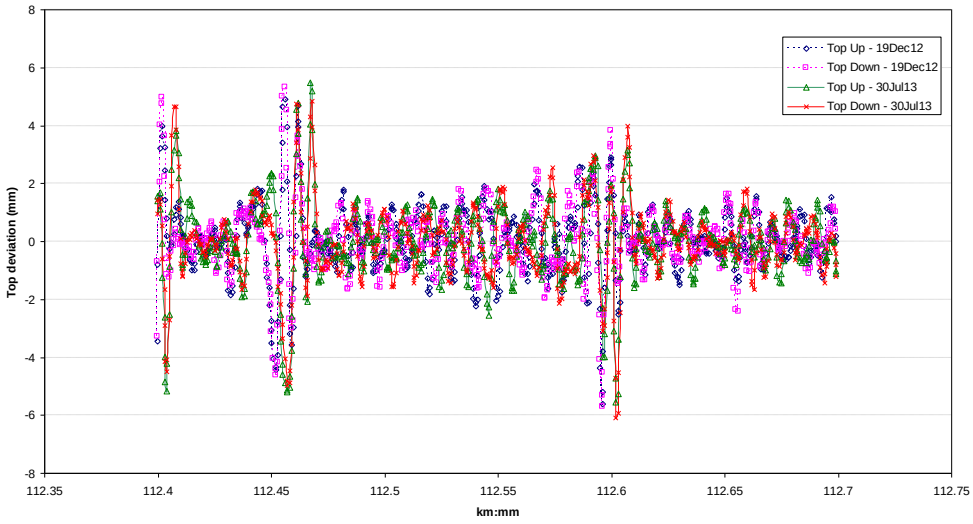


**Fig. 10.** Variation in track geometry data along the rail bridge after the construction of the transition zone [49]

In addition to these case studies, numerous experimental and numerical investigations have been conducted worldwide to investigate the benefits of using geocells. The subsequent sections discuss the influence of geocell on some of the parameters (or material properties) that are essential for the stability of a track.

# 4 Resilient modulus

## 4.1 Definition.

The resilient modulus is defined as the ratio of the cyclic deviator stress to the elastic vertical strain (resilient strain) during unloading [50]. It is expressed as:

$$Mr = \frac{\sigma_{cyc}}{{\epsilon_1}^e} \tag{11}$$

The resilient modulus is most commonly determined using the cyclic triaxial tests with a constant value of confining pressure and a cyclic variation of the deviator stress [51]. However, it is often very challenging to conduct the laboratory testing every-time before using the geo-material for rail or pavement application. Therefore, several models (based on the experimental investigations) have been developed that can be used to directly evaluate the value of resilient modulus at specific physical states, loading conditions and stress states [51].

### 4.2 **Resilient modulus vs Young's modulus.**

The resilient modulus of the granular material is often confused with Young's modulus. Although, both the terms measure the resistance against the elastic deformation, they may have significantly different applications. The resilient modulus is most commonly used to describe the behavior of granular materials under repeated loading. It is an essential parameter for the design of the pavements and the railway tracks [52].

The Young's modulus of a material is the ratio of the stress to the strain under loading, within the elastic limits. It is generally employed to describe the behavior of a material under monotonic loading conditions, and its value is constant for an isotropic material. The Young's modulus is the slope of the linear (elastic) portion of the stress-strain curve of the material, usually obtained from axial compression or tension tests. However, the soil (or granular material) often exhibit non-linear elastic behavior. Therefore, two Young's moduli are used to describe its response: initial Young's modulus ($E_i$) and secant Young's modulus ($E_{sec}$). The initial Young's modulus is the slope of the initial portion of the stress-strain curve, whereas, the secant modulus is the slope of the line joining the origin to a particular level of stress (or strain) in the stress-strain curve [53].

However, the behavior of the granular material (such as soil) may change significantly under the cyclic load. When a granular material is subjected to cyclic loading, the amount of deformation in each cycle includes a resilient component (recoverable) and a plastic component (irrecoverable) (Refer to Fig. 11). The resilient component for each cycle is calculated by subtracting the maximum strain under the peak load with the permanent strain after unloading. Initially, the amount of plastic strain increment is much higher than the resilient strain. However, with an increase in the number of cycles, the magnitude of plastic strain increment decreases. Subsequently, a stage is reached (known as shakedown) when the plastic strain increment diminishes, and the elastic strain becomes virtually constant [8]. The corresponding ratio of the deviator stress to the recoverable (elastic) strain at this stage is termed as the resilient modulus of the material. It must be noted that the variation of plastic strain with the number of cycles also depends on the stress levels. The plastic strain may increase continuously with an increase in the number of cycles at high deviator stress and low confining pressure [54].

The resilient modulus is usually determined after the completion of a number of cycles [8, 52]. However, it may also be calculated for each load cycle for the accurate prediction of the material behavior under repeated loads. The magnitude of the resili-

ent modulus (if calculated for each cycle) increases with an increase in the number of load cycles and becomes almost constant after a particular value. Moreover, the material becomes progressively stiffer with an increase in the number of load cycles [54]. Consequently, the magnitude of the resilient modulus of a material may even exceed Young's modulus.

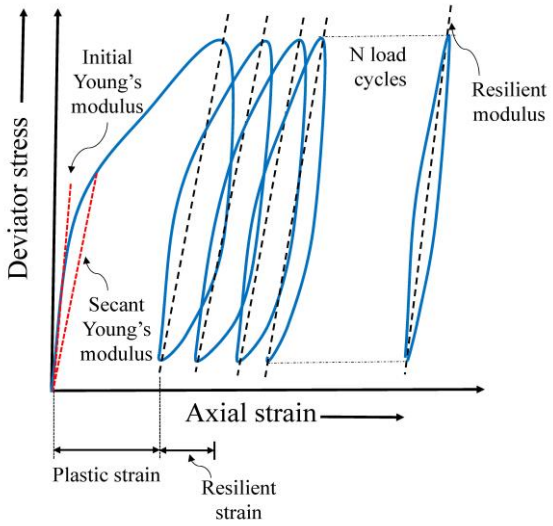


**Fig. 11.** Young's modulus and resilient modulus for soil

### 4.3 Resilient modulus vs. track modulus.

The track modulus is defined as the force per unit deflection per unit length of the track [32]. It is a measure of the resistance against deflection, produced by the track when a static wheel load is applied on the rail. In other words, track modulus is the static wheel load per unit length of the rail that is required to produce unit deflection in the track. The magnitude of the track modulus primarily depends on the properties of both the substructure and the superstructure, such as rail size, quality, dimensions and spacing of sleepers, quality and degree of compaction of ballast, sub-ballast and the subgrade [32]. Moreover, the train parameters such as speed and axle load also influence the magnitude of the track modulus [15].

The track modulus is a measure of the overall response of the railway track to a static wheel load whereas the resilient modulus is a measure of the response of a particular material layer (ballast, sub-ballast or subgrade) to repeated loading. In other words, track modulus is the property on a global level, whereas, the resilient modulus is the property of individual components.

### 4.4 Young's modulus vs. stiffness

The Young's modulus of a material is the ratio of the stress to the strain within the elastic limit. It is a measure of the resistance offered by a material to the elastic deformation under loading. It is a material property and doesn't depend on the shape and size of the material under loading. The unit of Young's modulus is identical to the units of stress, i.e. $N/m^2$.

Whereas, the stiffness of the material is a measure of the resistance offered by the material against deformation under loading. It depends on the shape and size of the material. The unit of stiffness is N/m.

### 4.5 Empirical models for resilient modulus.

Several empirical models have been developed for the prediction of resilient modulus for soil [51]. Table 2 discusses the different models.

**Table 2.** Empirical models for the prediction of resilient modulus

| Name | Model | Reference | Fitting parameters |
|---|---|---|---|
| Bilinear | $M_r = K_1 + K_2\sigma_d$, for $\sigma_d < \sigma_{di}$<br>$M_r = K_3 + K_4\sigma_d$, for $\sigma_d > \sigma_{di}$ | Thompson and Robnett [55] | $K_1$, $K_2$<br>$K_3$, $K_4$ |
| Power | $M_r = k^*{\sigma_d}^n$ | Moossazadeh and Witczak [56] | $k^*$, $n$ |
| Power | $M_r = k^*\left(\frac{\sigma_d}{\sigma'_3}\right)^n$, for saturated over-consolidated soils | Brown et al. [57] | $k^*$, $n$ |
| Semi-log | $M_r = 10^{(k^* - n\sigma_d)}$ | Fredlund et al. [58] | $k^*$, $n$ |
| Semi-log | $\log(M_r) = \left(k^* - n\frac{\sigma_d}{\sigma_{d(failure)}}\right)$ | Raymond et al. [59] | $k^*$, $n$ |
| Hyperbolic | $M_r = \frac{k^* + n\sigma_d}{\sigma_d}$ | Drumm [60] | $k^*$, $n$ |
| Octahedral | $M_r = k^*\left(\frac{\sigma_{oct}^n}{\tau_{oct}^m}\right)$ | Shackel [61] | $k^*$, m, $n$ |
| Stress-dependent | $M_r = k_1 P_a \left(\frac{\theta}{P_a}\right)^{k_2}\left(\frac{\tau_{oct}}{P_a} + 1\right)^{k_3}$ | Uzan [62] | $k_1$, $k_2$, $k_3$ ($k_1 > 0$, $k_2 \geq 0$ and $k_3 \leq 0$) |

Here, $\sigma_{di}$ is the deviator stress at which slope of the resilient modulus ($M_r$) vs. deviator stress ($\sigma_d$) curve changes; $\sigma'_3$ is the effective confining stress; $\sigma_{oct}$ and $\tau_{oct}$ are the octahedral normal and shear stresses respectively; $P_a$ is the atmospheric pressure; $\theta$ is the bulk stress.

The stress-dependent model given by Uzan [62] (Table 2) is the most commonly used method to evaluate the resilient modulus. The bulk and octahedral shear stresses in this model can be evaluated using the following set of equations:

$$\tau_{oct} = \frac{1}{3}\sqrt{(\sigma_1 - \sigma_2)^2 + (\sigma_1 - \sigma_3)^2 + (\sigma_2 - \sigma_3)^2} \quad (12)$$

$$\theta = \sigma_1 + \sigma_2 + \sigma_3 \quad (13)$$

where, $\sigma_1$, $\sigma_2$ and $\sigma_3$ are the major, intermediate and minor principal stresses, respectively. It is interesting to note that the stress-dependent model by Uzan [62] applies to both coarse-grained and fine-grained soils [52]. The model includes both the increment of resilient modulus with bulk stress and the reduction with an increase in the deviator stress for the coarse-grained and fine-grained soils respectively [55, 63].

The resilient modulus is a measure of the elastic stiffness of the geo-materials used for the construction of the track substructure [51]. Therefore, it can be used to predict the track performance (in terms of settlement) under repeated loads due to the rail traffic. Consequently, its study is essential for the design of the railway tracks. The resilient modulus of the soil depends on: i) the properties of the material such as type, gradation, degree of compaction, moisture content; ii) state of stress such as confining stress; and iii) the loading parameters such as magnitude, frequency, duration and the number of load cycles [51, 64].

### 4.6 Influence of geocell reinforcement on resilient modulus

Several researchers have conducted experimental and numerical investigations to understand the effect of geocell reinforcement on the resilient modulus of geomaterials. Some of the investigations are briefly discussed below.

**Experimental and field investigations.**

The geocell reinforcement generally improves the resilient modulus of the soil. However, the amount of improvement depends on the conditions, such as type of soil (fine-grained or coarse-grained), moisture content, confining pressure, deviator stress, frequency, number of load cycles, etc. [4, 63]. The experimental investigations by Edil and Bosscher [65] revealed that the resilient modulus of sand increases with confinement. Moreover, the field investigations by Al-Qadi and Hughes [66] on a pavement in Pennsylvania showed that the combination of geocell, geotextile and geogrid can improve the resilient modulus of the aggregates.

Mengelt et al. [63] conducted cyclic tri-axial tests to study the influence of geocell reinforcement on the resilient modulus and plastic deformation behavior of the soil. The use of geocell increased the resilient modulus by 1.4-3.2 % and 16.5-17.9 % for the coarse-grained and fine-grained soils respectively. Thus, the results indicated that the improvement is highly dependent on the soil type.

Tanyu et al. [26] conducted large-scale repeated load tests (in a 3 m × 3 m × 3.5 m reinforced concrete pit) on geocell reinforced gravel (which represents granular subbase layer for pavements). They observed a 40-50 % increase in the resilient modulus

on reinforcing the gravel with the geocell. Moreover, the increment was dependent on the thickness of the geocell reinforced layer. A higher degree of improvement was observed in thin layers as compared to thick layers.

Indraratna et al. [4] conducted repeated load tests on unreinforced and geocell reinforced sub-ballast under plain-strain condition. The use of plain-strain condition gave a realistic approach to investigate the behavior of the sub-ballast. The use of geocell increased the resilient modulus of the unreinforced sub-ballast by 10-18 %. Moreover, the resilient modulus for both the reinforced and unreinforced specimens increased (about 20 %) with an increase in the confining pressure and the loading frequency. Furthermore, the effect of frequency was more pronounced in the geocell reinforced specimens.

**Numerical and analytical investigations.**
Yang and Han [28] observed that the use of geocell increases the resilient modulus of Unbound Granular Material (UGM). The increase in resilient modulus increases non-linearly with an increase in the tensile stiffness and the cyclic deviator stress. Moreover, the improvement in resilient modulus decreases with an increase in the resilient modulus of the infill material and the confining pressure. Whereas, the improvement increases with a reduction in geocell pocket size and dilation angle of the infill material. Thus, the degree of improvement depends on the properties of both materials and the stress-state.

Liu et al. [48] studied the mechanical response of straight and curved geocell reinforced ballast embankment under monotonic and cyclic loading conditions using discrete element method (DEM). The results showed an increase in stiffness of the ballast bed under monotonic loading conditions and an increase in resilience under cyclic loading conditions.

# 5 Additional confinement

## 5.1 General.

The geocells provide an additional horizontal and vertical confinement to the infill material and restrain the upward movement of the base material (material below the geocell layer) outside the loaded area (mattress effect) [24, 67]. The horizontal confinement reduces the lateral deformation of the infill material. Moreover, the mattress effect results in a wider distribution of vehicle load and thus prevents excessive deformation (or failure) in soft subgrades [24].

However, the amount of confinement depends on the properties of the geocell and the loading conditions. Yang and Han [28] observed that the additional confining pressure provided by the geocell reinforcement decreases with an increase in the geocell pocket size. This reduction is because the quantity of geocell material that reinforces the infill decreases with an increase in pocket size.

Moreover, the plain strain cyclic loading tests by Indraratna et al. [4] revealed that the loading frequency and external confining pressure significantly affect the addi-

tional confinement provided by the geocell. The additional confinement increased with an increase in loading frequency. However, it decreased with an increase in the external confining pressure at a particular loading frequency.

### 5.2 Models to quantify additional confinement.

The confinement provided by the geocells to the infill is identical to the confinement provided by the membrane to the soil sample in a triaxial test. Therefore, the magnitude of additional confinement can be evaluated using the classical work of Henkel and Gilbert [68]. Henkel and Gilbert [68] quantified the additional confinement provided by the membrane (in a triaxial test) and its influence on the shear strength of the soil [63].

Tanyu et al. [26] used the theory developed by Henkel and Gilbert [68] to evaluate the additional confining stress produced by the geocells on the soil (Eq. 14). The geocell strain data collected from the experiments were used in the Eq. 14 to determine the additional confining stress.

$$\Delta\sigma_3 = \frac{2M\varepsilon_c}{d(1-\varepsilon_a)} \tag{14}$$

where, $M$ is the modulus of the membrane (or geocell); $\varepsilon_a$ is the axial strain of the specimen (soil); $d$ is the diameter of the specimen; $\varepsilon_c$ is the circumferential strain.

$$\varepsilon_c = \frac{1-\sqrt{1-\varepsilon_a}}{\sqrt{1-\varepsilon_a}} \tag{15}$$

Yang and Han [28] developed an analytical model to predict the additional confinement provided by the geocell in the repeated load triaxial tests. They suggested that the hoop stress developed in the geocell generates additional confining pressure within the infill material. Moreover, they assumed a uniform distribution of hoop stress along the height of the geocell. The additional confining pressure due to the incorporation of geocell was mathematically represented as (Eq. 16):

$$\Delta\sigma_3 = \frac{M_t}{D}\left[\frac{-\Delta\sigma_3}{M_{r1}} + \frac{\sigma_1-(\sigma_3+\Delta\sigma_3)}{M_{r2}}\right]\left\{\frac{\varepsilon_0}{\varepsilon_r}\right\} e^{\left(-\frac{\rho}{N_{limit}}\right)^{\beta}}\left(\frac{1+sin\psi}{1-sin\psi}\right) \tag{16}$$

where, $\Delta\sigma_3$ is the additional confining stress due to geocell; $M_t$ is the tensile stiffness of the geocell; $D$ is the diameter of the sample; $\psi$ is the dilation angle; $\sigma_1$ and $\sigma_3$ are the major and minor principal stresses; $\varepsilon_0/\varepsilon_r$, $\rho$ and $\beta$ are the fitting parameters for the permanent deformation test curve of UGM; $N_{lim}$ is the number of load repetitions required to reach the resilient state; $M_{r1}$ and $M_{r2}$ are the resilient modulus of the granular material corresponding to first and second stages of repeated load triaxial tests respectively. The first stage corresponds to the condition when the axial stress increases from $\sigma_3$ to $\sigma_3+\Delta\sigma_3$. The second stage corresponds to the increase of axial stress from $\sigma_3+\Delta\sigma_3$ to $\sigma_1$.

However, Yang and Han [28] ignored the influence of loading frequency on the additional confining pressure. Furthermore, the resilient modulus and dilation angle

vary with the number of loading cycles [4]. Therefore, using a constant value of resilient modulus and dilation angle can limit the accuracy of the proposed model.

Indraratna et al. [4] derived a semi-empirical model using hoop tension theory, to determine the additional confinement provided by the geocell to an infill under the plain-strain loading condition. They also incorporated the influence of loading frequency and load cycles on the mobilized modulus of geocell and the mobilized dilation angle for infill material. This was done by varying the mobilized geocell modulus and mobilized dilation angle in accordance with the strain reached during a particular loading cycle. The additional confinement was calculated as (Eq. 17):

$$\Delta\sigma'_3 = \int_{N_l=1}^{N_l=N_{lim}} \left[\frac{2M_m}{D_g}\left\{\frac{(1-\mu_g)\mathrm{k}'+\mu_g}{(1+\mu_g)(1-2\mu_g)}\right\}\left\{\frac{-\mu_g\sigma_{cyc}}{dM_r} + d\varepsilon_{1,1}^{p}\left(\frac{a'}{N_l}+\frac{b'}{N_l}\right)\left(\frac{1+\sin\psi_m}{1-\sin\psi_m}\right)\right\}\right] dN_l \quad (17)$$

where, $\Delta\sigma_3^{'}$ is the additional confining pressure; $N_l$ is the number of load cycles; $N_{lim}$ is the number of cycles required to reach a stable zone; $M_m$ and $\mu_g$ are the mobilized modulus and the Poisson's ratio of the geocell, respectively; $k'$ is the ratio of circumferential strain to the radial strain in geocell; $D_g$ is the diameter of the geocell opening (the geocell opening is assumed circular); $\sigma_{cyc}$ is the cyclic deviator stress; $M_r$ is the resilient modulus of infill; $\varepsilon_{1,1}^{p}$ is the permanent axial strain after the first load cycle; $a^{'}$ and $b^{'}$ are the empirical coefficients; $\psi_m$ is the mobilized dilation angle.

The semi-empirical model given by Indraratna et al. [4] can be further improved to evaluate the additional confinement provided by the geocell under quasi-three-dimensional loading condition. Figs. 12 (a) and (b) show the deformation profile of a geocell under quasi-three-dimensional and plain-strain loading conditions respectively.

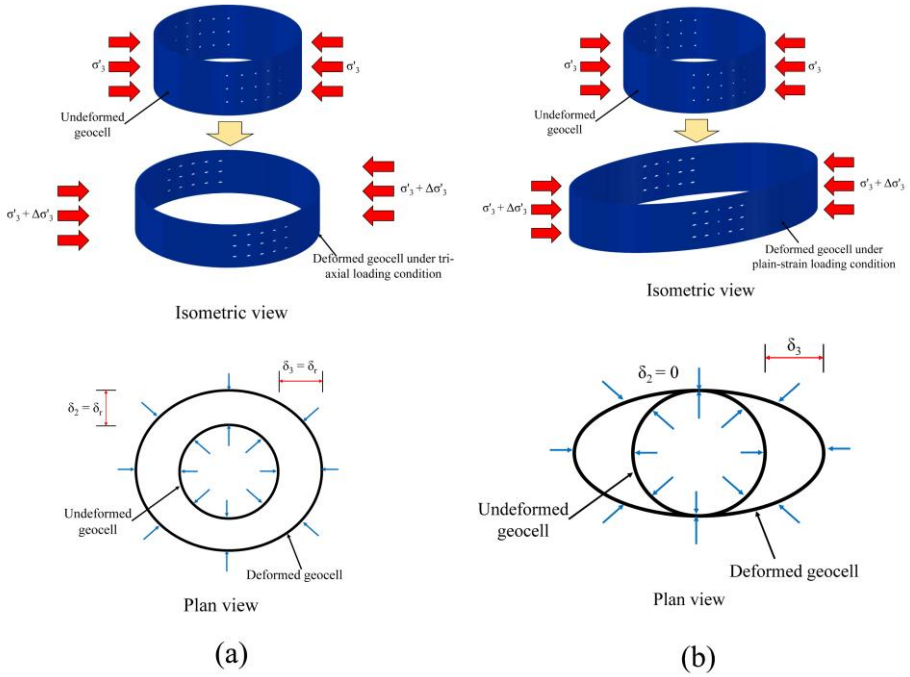


**Fig. 12.** Deformation of geocell under (a) triaxial loading condition (b) plain-strain loading condition

It is assumed that the geocell deforms as a right circular cylinder under the quasi-three-dimensional loading conditions. In other words, the deformation is uniform along the height of the geocell. However, in the plain-strain condition, the geocell deforms into an elliptical cylinder. The deformation in the geocell produces circumferential stress. This circumferential stress provides additional confinement to the infill.

Thus, the additional confining pressure provided by a single geocell pocket is given by:

$$\Delta\sigma'_3 = \frac{2\sigma_c}{D_g} \tag{18}$$

where, $\sigma_c$ is the circumferential stress in the geocell. The circumferential stress in the geocell can be evaluated using the Hooke's law:

$$\sigma_c = M_m \left[\frac{(1-\mu_g)\varepsilon_c + \mu_g(\varepsilon_3+\varepsilon_z)}{(1+\mu_g)(1-2\mu_g)}\right] \tag{19}$$

where, $\varepsilon_c$, $\varepsilon_3$ and $\varepsilon_z$ are the circumferential, radial and vertical strains respectively. For multiple geocells (entire geocell mattress), the Eq. 18 can be modified to:

$$d(\Delta\sigma'_3) = \frac{2M_m}{D_g}\left[\frac{(1-\mu_g)\mathrm{k}'+\mu_g}{(1+\mu_g)(1-2\mu_g)}\right](-d\varepsilon_3) \tag{20}$$

The radial strain rate can be expressed as the sum of elastic and plastic components (Eq. 21):

$$d\varepsilon_3 = d\varepsilon_3^e + d\varepsilon_3^p \tag{21}$$

$$d\varepsilon_3^e = \frac{\mu_g \sigma_{cyc}}{dM_r} \tag{22}$$

where, $\sigma_{cyc}$ is the cyclic deviator stress; $M_r$ is the resilient modulus of infill. The plastic component of radial strain rate can be evaluated using the dilatancy equation [69].

$$\sin\psi_m = -\frac{\mathrm{d}\varepsilon_1^p + x\,\mathrm{d}\varepsilon_3^p}{\mathrm{d}\varepsilon_1^p - x\,\mathrm{d}\varepsilon_3^p} \tag{23}$$

where, $\psi_m$ is the mobilized dilation angle; $d\varepsilon^p{}_1$ and $d\varepsilon^p{}_3$ are the plastic axial strain rate and plastic lateral strain rate respectively; $x$ is 2 for triaxial test condition [70].

Thus, the plastic strain rate becomes:

$$d\varepsilon_3{}^p = \left[-\frac{d\varepsilon_1^p}{2}\left(\frac{1+\sin\psi_m}{1-\sin\psi_m}\right)\right] \tag{24}$$

Combining Eq. 21, 22 and 24, the radial strain rate can be expressed as:

$$d\varepsilon_3 = \left[\frac{\mu_g\sigma_{cyc}}{dM_r} - \frac{d\varepsilon_1^p}{2}\left(\frac{1+\sin\psi_m}{1-\sin\psi_m}\right)\right] \tag{25}$$

The variation of additional confining pressure for the complete geocell mattress with the number of load cycles can be expressed by considering the relationship between permanent vertical strain and number of load cycles [13] (discussed later in Eq. 29). Thus, the additional confinement due to the overall geocell mattress can be evaluated by the following expression:

$$\Delta\sigma'_3 = \int_{N_l=1}^{N_l=N_{lim}}\left[\frac{2M_m}{D_g}\left\{\frac{(1-\mu_g)\mathrm{k}'+\mu_g}{(1+\mu_g)(1-2\mu_g)}\right\}\left\{\frac{-\mu_g\sigma_{cyc}}{dM_r} + \frac{d\varepsilon_{1,1}^p}{2}\left(\frac{a'}{N_l}+\frac{b'}{N_l}\right)\left(\frac{1+\sin\psi_m}{1-\sin\psi_m}\right)\right\}\right]dN_l \tag{26}$$

# 6 Plastic deformation

## 6.1 General.

The long-term performance of a railway track depends on the plastic response of its constituent materials, i.e., the ballast, sub-ballast and subgrade soil. The excessive plastic deformation of the soil subgrade or the granular layers (ballast and sub-ballast) under repeated traffic loads is detrimental for the stability of a rail track. It demands frequent maintenance cycles and also leads to poor riding quality which decreases the passenger comfort [71].

The granular materials usually tend to densify under the application of cyclic or repeated loading [12, 13]. This densification is due to the reorientation and rearrangement of the particles, and also due to the particle breakage in response to the repeated loading. This response leads to permanent deformation in the track, and consequently, the track efficiency decreases. Nevertheless, the plastic response of the granular materials depends on a large number of factors such as [54]:

- Stress levels – plastic deformation is directly proportional to the deviator stress and inversely proportional to the confining pressure.
- Principal stress rotation - leads to larger permanent strain than those predicted by cyclic tri-axial tests
- Number of load cycles
- Moisture content – plastic deformation may increase due to excessive positive pore water pressure or lubrication
- Density – deformation decreases with an increase in density
- Stress history
- Grading, type of aggregate and fine content

### 6.2 Influence of geocell reinforcement on plastic deformation.

Pokharel et al. [67] conducted monotonic and repeated plate load tests on the sand and reported that the geocell reinforcement reduces the permanent deformation, and increases the stiffness and bearing capacity. Moreover, the moving wheel test conducted by Pokharel et al. [24] revealed that the geocell reinforcement increases the confinement in infill and distributes the load over a wide area, which results in a reduction in subgrade stress and deformation.

The studies by Yang and Han [28] revealed that the geocell reinforcement reduces the permanent deformation of the UGM. Moreover, they observed that the reduction in permanent deformation due to geocell reinforcement depends on the external confining pressure, tensile stiffness and the opening size of the geocell. The reduction in permanent deformation

- Increases non-linearly with an increase in the tensile stiffness of geocell.
- Increases with a reduction in geocell size.
- Increases with an increase in the dilation angle of the infill.
- Decreases with an increase in the resilient modulus of the infill.
- Decreases with an increase in confining pressure and cyclic deviator stress.

Leshchinsky and Ling [29] conducted a series of model tests to investigate the influence of the number and location of the geocell layers on the strength and stiffness of an embankment of poorly graded gravel. The poorly graded gravel embankment was assumed representative of the ballast bed in railways. The gravel embankment was loaded both monotonically and cyclically, and results of the tests with and without geocell reinforcement were compared. The experimental results showed that the reinforcement of gravel with geocell significantly reduces the vertical settlement and lateral deformation in both monotonic and repeated loading tests. Interestingly, the results showed that the maximum amount of lateral spreading occurred just above the

geocell layer. Subsequently, a parametric study was conducted using finite element analysis to investigate the influence of geocell stiffness, type of subgrade, and strength of gravel on the behavior of geocell reinforced gravel embankment. The results showed that the subgrade stress reduced significantly with an increase in the geocell stiffness. However, the magnitude of stress reduction depends on the stiffness of the subgrade. No significant reduction was observed for a stiff subgrade. Conversely, the settlement reduced considerably for the stiff subgrade. Thus, the authors argued that the geocell might have a beneficial effect on both the soft and stiff subgrade.

Leshchinsky and Ling [21] used 3D finite element analyses to investigate the behavior of ballasted railway track with and without geocell reinforcement under monotonic loading. The results showed that the reinforcement of ballast by geocell significantly reduces the vertical settlement of the track. However, the amount of reduction depends on the stiffness of geocell and subgrade in addition to the ballast strength. The decrease in the vertical settlement was more effective in case of soft or stiff subgrade, however, in very soft subgrade, there was a little benefit. This effect was probably due to the tendency of the ballast to undergo a significant amount of lateral deformation when a stiff subgrade underlies it. The geocell prevents this lateral deformation and hence, reduces the vertical settlement of the track. Moreover, the geocell stiffness had little influence on the vertical settlement and lateral deformation of the ballasted track. Furthermore, the decrease in settlement and lateral deformation was more significant for low strength ballast as compared to high strength ballast on soft subgrades.

The experimental investigation by Indraratna et al. [4] showed that the addition of geocells in the sub-ballast layer decreases the permanent axial strain. Moreover, this beneficial role of geocell was more pronounced at low confining pressures (5-10 kPa). Furthermore, the reduction in permanent axial strain increased with an increase in the loading frequency.

Satyal et al. [18] conducted cyclic plate load tests, and 3-D finite element analyses on geocell reinforced ballast over soft subgrade to assess the beneficial role of geocell in the railway tracks. They observed that the geocell reinforced ballast layer distributes the traffic induced load uniformly to a wide area in the soil subgrade and consequently, reduces the plastic deformation. Moreover, the strain in the geocell was within the elastic range, and no significant damage was observed in geocells. Subsequently, they validated the numerical results with the experimental plate load tests and then conducted a parametric study. The parametric studies showed an overall 30% reduction in track settlement on reinforcing the ballast by geocell. Moreover, the amount of settlement reduction was dependent on the position and number of geocell layers. The use of two geocell layers one above the other produced the least settlement. Further, the effectiveness of geocell reinforcement decreased with an increase in the strength of subgrades.

The DEM analyses of geocell reinforced straight, and curved embankments by Liu et al. [48] showed that the application of geocell significantly reduce the vertical deformation of ballasted embankment under both monotonic and cyclic loading. This effect was more pronounced if the layer was placed at some distance above the sub-

grade. Moreover, it was observed that at the initial stages of monotonic loading, the geocell confinement was not mobilized and both the unreinforced and reinforced embankments showed similar stiffness. However, after a particular value of the load, the stiffness of geocell reinforced embankment increased. The ballast inside the infill tends to move downwards, however, the ballast for unreinforced case tends to move sideways in addition to the vertical movement.

Furthermore, the repeated plate loading tests by Pokharel et al. [25] showed that the use of geocell reduces the permanent deformation of a layer as compared to the unreinforced case.

### 6.3 Prediction of plastic deformation.

Several mathematical models are available to predict the plastic deformation of the soil subgrade and the granular layers under repeated loading. Some of the models are discussed below:

Li and Selig [71] gave a power model to predict the cumulative plastic deformation in fine-grained subgrade soils under repeated loading. The model considered the influence of the number of load cycles, and the type, stress state (deviator stress) and physical state (dry density and moisture content) of the soil on the cumulative plastic strain (Eq. 27).

$$\varepsilon_p = a' \left(\frac{\sigma_d}{\sigma_s}\right)^{m^*} N_l{}^b \tag{27}$$

where, $a'$, $m^*$ and $b$ are the material parameters; $N_l$ is the number of load cycles; $\sigma_s$ and $\sigma_d$ are the static shear strength of the soil and deviator stress respectively; $\varepsilon_p$ is the cumulative plastic strain. The static shear strength of the soil represents the influence of the physical state on the cumulative plastic strain (and to some extent on the structure of the soil). The parameters $a'$, $m^*$ and $b$ depend on the type of soil and their average values vary between 0.64-1.2, 1.7-2.4 and 0.1-0.18 respectively for fine-grained soils (ML, MH, CL and CH (Unified soil classification system)) [71].

Yang and Han [28] proposed an analytical model to evaluate the permanent deformation of geocell reinforced UGM under repeated load triaxial test condition when it reaches the resilient state.

$$\varepsilon_1{}^p = \left[-\frac{\Delta\sigma_3}{M_{r1}} + \frac{\sigma_1-(\sigma_3+\Delta\sigma_3)}{M_{r2}}\right]\left(\frac{\varepsilon_0}{\varepsilon_r}\right) e^{-(\rho/N_{lim})^\beta} \tag{28}$$

where, $\varepsilon_1{}^p$ is the permanent axial strain. The other parameters have the same meaning as in Eq. 16. Thus, to evaluate the permanent axial deformation, the additional confining pressure due to geocell need to be evaluated. The parameters $M_{r1}$ and $M_{r2}$ can be calculated using the equations in Table 2.

Indraratna and Nimbalkar [13] proposed a model to evaluate the variation of permanent axial strain in the ballast with the number of load cycles (Eq. 29).

$$\varepsilon_1{}^p = \varepsilon_{1,1}{}^p(1 + a^* \ln N_l + 0.5b^* (\ln N_l)^2) \tag{29}$$

An attempt has been made to predict the variation of permanent deformation with the number of load cycles for different types of infill (for both unreinforced and geocell reinforced cases). The experimental data from the cyclic plate load tests conducted by different researchers were used to derive the empirical coefficients $a^*$ and $b^*$. The permanent deformation was then predicted using the Eq. 29. The accuracy of the coefficients was then evaluated by comparing the back-fitted data with the experimental data. Table 3 gives the values of empirical coefficients/ model parameters obtained for the unreinforced and geocell-reinforced cases.

**Table 3.** Model parameters to predict permanent deformation

| S. no. | Reference | Infill | Condition | Model parameters | |
|---|---|---|---|---|---|
| | | | | $a^*$ | $b^*$ |
| 1 | Thakur et al. [72] | Recycled asphalt pavement (RAP) | Unreinforced | 0.148 | 1.820 |
| 2 | Thakur et al. [72] | RAP | Geocell reinforced | 0.155 | 0.591 |
| 3 | Leshchinsky and Ling [29] | Gravel | Unreinforced embankment | 32.89 | 6.459 |
| 4 | Leshchinsky and Ling [29] | Gravel | Geocell reinforced embankment (single layer) | 0.1 | 122.5 |
| 5 | Tanyu et al. [26] | Grade-2 gravel | Unreinforced | 0.05 | 0.68 |
| 6 | Tanyu et al. [26] | Grade-2 gravel | Reinforced (geocell with 200 mm diameter and 200 mm height) | 1.386 | 0.461 |
| 7 | Pokharel et al. [25] | Aggregate base type 3 (AB-3) | Unreinforced (Maximum applied pressure - 552 kPa) | 0.217 | 0.026 |
| 8 | Pokharel et al. [25] | AB-3 | Geocell reinforced (single cell, maximum applied pressure - 552 kPa) | 0.146 | 0.079 |
| 9 | Pokharel et al. [25] | AB-3 | Geocell reinforced (multiple cells, maximum applied pressure - 552 kPa) | 0.415 | 0.050 |

Fig. 13 shows the experimental vs. predicted results for the tests conducted by [25, 26, 29, 72]. The permanent deformation has been normalized with the layer/specimen thickness to allow the comparison of results from the different studies. The figure shows that for all the cases, the geocell reinforcement significantly reduced the permanent deformation or settlement of the infill. Moreover, the results from model predictions are in close agreement with the experimental results.

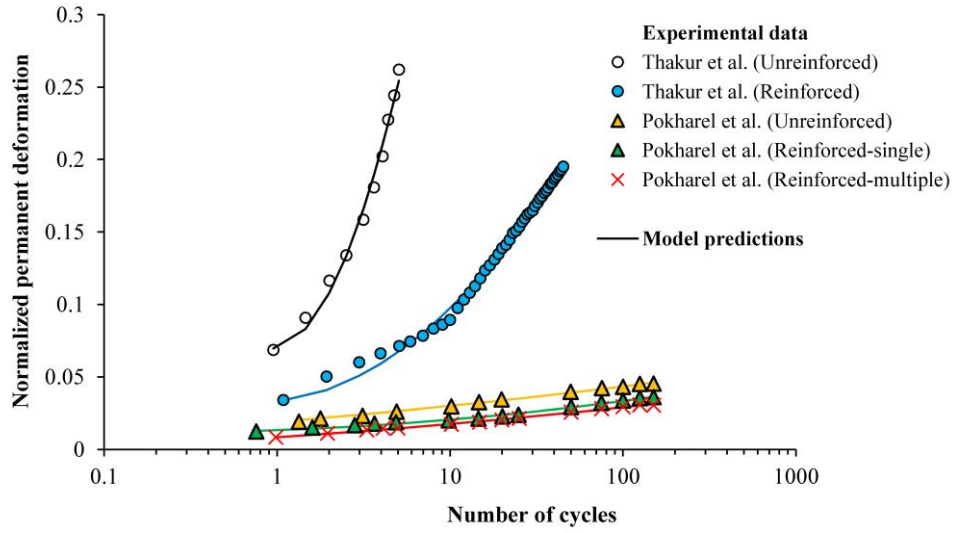


(a)

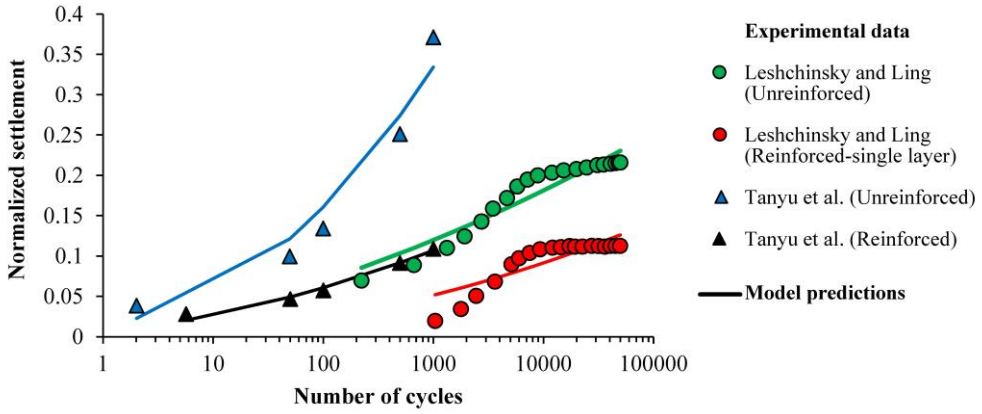


(b)

**Fig. 13.** Comparison of predicted and experimental results from previous studies

## 7 Factors affecting geocell applications in railways (can be removed)

The following factors may affect the application of geocells in the railway tracks:

### 7.1 Geocell properties.

The stiffness, size, shape, seam strength are some of the properties that may influence the performance of the geocell. The stiffness of geocell is crucial for the long-term stability and the overall cost of the reinforced track. The use of stiffer materials usually improves the confinement. However, the stiffer materials may be more expensive as compared to the soft materials. Moreover, large strains are generated in the soft material as compared to the rigid material for the same amount of vertical load.

The shape of geocell significantly influences the response of the geocell reinforced layer. The layers with elliptical geocells are less stiff as compared to the layers with circular geocells [23]. Furthermore, the performance of geocell reinforced layer decreases with an increase in the geocell pocket size.

The seam strength of geocells also plays a vital role in the long-term performance of the geocell reinforced tracks. The geocell reinforced layer behaves identical to a slab that bends and distributes the vertical load uniformly over a wide area. Due to bending, high tensile stresses are generated near the bottom portion of the geocell layer [29]. These stresses may exceed the seam strength (which is usually smaller than the tensile strength) and lead to wear and tear in the geocell. This wear and tear ultimately reduce the service life of geocell.

### 7.2 Subgrade stiffness and strength.

The subgrade strength and stiffness play an essential role in the behavior of the geocell reinforced track. The total deformation in a railway track can be divided into two components ballast deformation (or sub-ballast deformation) and the subgrade deformation [32]. For soft subgrades, the contribution of subgrade deformation is much higher as compared to the ballast deformation. Conversely, for the stiff soils, the contribution of ballast deformation is significant. For stiff soils, the ballast (or sub-ballast) layer tends to deform laterally which leads to the vertical deformation of the track. The geocells can significantly improve the performance of the track in this case by providing additional confinement to the ballast and reducing the lateral deformation. Moreover, for soft soils, the geocells distribute the loads over a wider area and reduce the subgrade stress. Consequently, the settlement of subgrade decreases.

Furthermore, the subgrade stiffness influences the magnitude of strain developed in the geocell. A large amount of strain is developed in the geocell for very soft subgrades as compared to the soft subgrades [21].

### 7.3 Properties of infill materials.

The performance of a geocell reinforced layer also depends on the properties of the infill. Pokharel [23] observed that the geocell confinement provides an apparent cohesion to the infill material. Therefore, the benefit of using geocell reduces if the infill material contains a significant amount of cohesion. Conversely, repeated plate load tests by Pokharel et al. [25] showed that the geocell reinforcement reduces the cumulative deformation in infill with fine as compared to the unreinforced case.

The benefit of using geocell increases with an increase in the dilation angle of the infill. However, the use of high strength materials as infill decreases the beneficial role of geocell.

### 7.4 Geocell location.

The geocell reinforced layer can be provided at the ballast bed, sub-ballast bed or above the soil subgrade. As discussed in the previous sections, the beneficial role of geocell decreases with an increase in the depth of geocell placement from the top of the track. However, the geocell cannot be used at the top of the ballast bed due to a high magnitude of vertical stresses and also due to the track maintenance requirements. Moreover, the use of multiple layers in the ballast bed can further improve the track stability. However, this effect is negligible for high strength ballast [29].

## 8 Conclusions

The present chapter examined the potential for the use of geocells in the railway tracks. The following conclusions may be drawn from the present chapter:

- The geocell confinement significantly improves the strength and stiffness of the granular infill materials. Therefore, the geocells can be used in the conventional ballasted tracks to confine the ballast or the sub-ballast layers. The confinement would reduce the track deformations in both lateral and vertical directions. Moreover, the geocell reinforced ballast (or sub-ballast) layer would behave as a rigid slab and distribute the train-induced loads uniformly over a wide area of the subgrade. Consequently, the settlement in the subgrade would reduce and the track geometry would be retained over an extended period.
- The geocells can be provided in the transition zones near the railway bridges to increase the stiffness of the track gradually. This increase in track stiffness would reduce the magnitude of the impact loads near the bridge ends and prevent the track geometry degradation.
- The geocells increase the strength and resilience of the geo-materials under the cyclic loading. However, the amount of improvement depends on the properties of geocell, infill and the loading conditions such as frequency and magnitude of the vertical load.
- The geocell reinforcement may decrease the amount and rate of plastic deformation in the track. This effect is beneficial for maintaining the track geometry over an extended period and reduce the frequency of maintenance cycles. However, the reduction in permanent deformation depends on several parameters such as the magnitude and frequency of load, properties of infill and the properties of the geocell.
- Several analytical models have been developed to evaluate the increase in confining pressure due to geocell reinforcement. These models can be used effectively for the design of geocell reinforced layers.

- The performance of a geocell reinforced layer depends on the properties of the infill, subgrade, location of the layer within the track and the loading conditions. A thorough analysis of these parameters is essential for the selection of a suitable type of geocell.

Thus, the geocell reinforcement possesses enormous applications in the railway tracks. However, the development of design guidelines at the present stage is difficult due to a limited number of studies that focus on the use of geocells in the railways. Nevertheless, the guidelines such as ARTC RTS 3430 [73] have recommended the use of geocell immediately below the ballast layer for the stabilization of the subgrade with a CBR value of 1 or less. This recommendation indicates a potentially bright future of the geocells in the field of railway geotechnics.

## Acknowledgement

The last author wishes to thank the European Commission for H2020-MSCA-RISE, Project No. 691135 “RISEN: Rail Infrastructure Systems Engineering Network”, which enables a global research network that tackles the grand challenge in railway infrastructure resilience and advanced sensing (www.risen2rail.eu) [74].

## References

1. Ngamkhanong, C. and S. Kaewunruen, *The effect of ground borne vibrations from high speed train on overhead line equipment (OHLE) structure considering soil-structure interaction.* Sci Total Environ, 2018. **627**: p. 934-941.
2. Connolly, D.P., et al., *Benchmarking railway vibrations – Track, vehicle, ground and building effects.* Construction and Building Materials, 2015. **92**: p. 64-81.
3. Indraratna, B., Y. Sun, and S. Nimbalkar, *Laboratory Assessment of the Role of Particle Size Distribution on the Deformation and Degradation of Ballast under Cyclic Loading.* Journal of Geotechnical and Geoenvironmental Engineering, 2016. **142**(7).
4. Indraratna, B., M.M. Biabani, and S. Nimbalkar, *Behavior of Geocell-Reinforced Subballast Subjected to Cyclic Loading in Plane-Strain Condition.* Journal of Geotechnical and Geoenvironmental Engineering, 2015. **141**(1).
5. Powrie, W., *On track: the future for rail infrastructure systems.* Proceedings of the Institution of Civil Engineers - Civil Engineering, 2014. **167**(4): p. 177-185.
6. Krylov, V.V., *Noise and vibration from high-speed trains*. Noise and vibration from high-speed trains. 2001.
7. Indraratna, B., W. Salim, and C. Rujikiatkamjorn, *Advanced Rail Geotechnology – Ballasted Track*. 2011, Balkema: CRC Press.
8. Selig, E.T. and J.M. Waters, *Track geotechnology and substructure management*. 1994, London: Thomas Telford.

9. Nimbalkar, S., et al., *Improved Performance of Railway Ballast under Impact Loads Using Shock Mats.* Journal of Geotechnical and Geoenvironmental Engineering, 2012. **138**(3): p. 281-294.
10. Sun, Q.D., B. Indraratna, and S. Nimbalkar, *Effect of cyclic loading frequency on the permanent deformation and degradation of railway ballast.* Géotechnique, 2014. **64**(9): p. 746-751.
11. Indraratna, B. and W. Salim, *Deformation and degradation mechanics of recycled ballast stabilised with geosynthetics.* Soils and Foundations, 2003. **43**(4): p. 35-46.
12. Indraratna, B., et al., *Field assessment of the performance of a ballasted rail track with and without geosynthetics.* Journal of Geotechnical and Geoenvironmental Engineering 2010. **136**(7): p. 907-917.
13. Indraratna, B. and S. Nimbalkar, *Stress-strain degradation response of railway ballast stabilized with geosynthetics* Journal Of Geotechnical And Geoenvironmental Engineering, 2013. **139**(5): p. 684-700.
14. Indraratna, B., S. Nimbalkar, and T. Neville, *Performance assessment of reinforced ballasted rail track.* Proceedings of the ICE: Ground Improvement, 2014. **167**(1): p. 24-34.
15. Nimbalkar, S. and B. Indraratna, *Improved performance of ballasted rail track using geosynthetics and rubber shockmat.* Journal of Geotechnical and Geoenvironmental Engineering, 2016. **142**(8).
16. Koerner, R.M., *Designing with geosynthetics*. Vol. 1. 2012: Xlibris Corporation.
17. Li, D. and E.T. Selig, *Method for railroad track foundation design. II: Applications.* Journal of Geotechnical and Geoenvironmental Engineering, 1998. **124**(4): p. 323-329.
18. Satyal, S.R., et al., *Use of cellular confinement for improved railway performance on soft subgrades.* Geotextiles and Geomembranes, 2018. **46**(2): p. 190-205.
19. Raymond, G.P., *Failure and reconstruction of a gantry crane ballasted track.* Canadian geotechnical journal, 2001. **38**(3): p. 507-529.
20. Zarembski, A.M., et al., *Application of Geocell Track Substructure Support System to Correct Surface Degradation Problems Under High-Speed Passenger Railroad Operations.* Transportation Infrastructure Geotechnology, 2017. **4**(4): p. 106-125.
21. Leshchinsky, B. and H.I. Ling, *Numerical modeling of behavior of railway ballasted structure with geocell confinement.* Geotextiles and Geomembranes, 2013. **36**: p. 33-43.
22. Bathurst, R.J. and R. Karpurapu, *Large-scale triaxial compression testing of geocell-reinforced granular soils.* Geotechnical Testing Journal, 1993. **16**(3): p. 296-303.
23. Pokharel, S.K., et al., *Investigation of factors influencing behavior of single geocell-reinforced bases under static loading.* Geotextiles and Geomembranes, 2010. **28**(6): p. 570-578.
24. Pokharel, S.K., et al., *Accelerated pavement testing of geocell-reinforced unpaved roads over weak subgrade.* Transportation Research Record, 2011. **2204**(1): p. 67-75.
25. Pokharel, S.K., et al., *Experimental evaluation of geocell-reinforced bases under repeated loading.* International Journal of Pavement Research and Technology, 2018. **11**(2): p. 114-127.

26. Tanyu, B.F., et al., *Laboratory evaluation of geocell-reinforced gravel subbase over poor subgrades.* Geosynthetics International, 2013. **20**(2): p. 47-61.
27. Giroud, J. and J. Han, *Design method for geogrid-reinforced unpaved roads. II. Calibration and applications.* Journal of Geotechnical and Geoenvironmental Engineering, 2004. **130**(8): p. 787-797.
28. Yang, X. and J. Han, *Analytical Model for Resilient Modulus and Permanent Deformation of Geosynthetic-Reinforced Unbound Granular Material.* Journal of Geotechnical and Geoenvironmental Engineering, 2013. **139**(9): p. 1443-1453.
29. Leshchinsky, B. and H. Ling, *Effects of Geocell Confinement on Strength and Deformation Behavior of Gravel.* Journal of Geotechnical and Geoenvironmental Engineering, 2013. **139**(2): p. 340-352.
30. Esveld, C., *Modern railway track*. 2001, Delft, The Netherlands: MRT-Productions.
31. Remennikov, A.M. and S. Kaewunruen, *A review of loading conditions for railway track structures due to train and track vertical interaction.* Structural Control and Health Monitoring, 2008. **15**(2): p. 207-234.
32. Doyle, N.F., *Railway track design a review of current practice*, B.o.t. economics, Editor. 1980, Australian government publishing service: Canberra.
33. Sayeed, M.A. and M.A. Shahin, *Three-dimensional numerical modelling of ballasted railway track foundations for high-speed trains with special reference to critical speed*. Transportation Geotechnics, 2016. **6**: p. 55-65.
34. Prause, R.H., et al., *Assessment of design tools and criteria for urban rail track structures*. 1974, Urban Mass Transportation Administration: Washington, DC.
35. AREA, *Manual of recommended practice*, A.R.E. Association, Editor. 1978: Washington D.C., USA.
36. Eisenmann, J., *Germans gain a better understanding of track structure.* Railway Gazette International, 1972. **128**(8).
37. ORE, *Stresses in the rails*. 1968: Utrecht.
38. Atalar, C. *Settlement of geogrid-reinforced railroad bed due to cyclic load*. in *Proc. 15th Int. Conf. on Soil Mech. and Geothch. Engrg.* 2001.
39. Board, B.R., *Permissible track forces for railway vehicles*. 1993, Group Standards, Railway Technical Centre: Derby.
40. Board, B.R., *Commentary On Permissible Track Forces for Railway Vehicles*, in *Technical Commentary*. 1995, Safety & Standards Directorate, Railtrack Railway Technical Centre, London Road. p. 9.
41. Indraratna, B., et al., *Performance improvement of rail track substructure using artificial inclusions – Experimental and numerical studies.* Transportation Geotechnics, 2016. **8**: p. 69-85.
42. Rail Safety and Standards Board, *Permissible track forces for railway vehicles. Group Standard GM/TT0088, Issue 1, Revision A*
in *Group Standard GM/TT0088, Issue 1, Revision A*. 1993, Rail Safety and Standards Board: London.
43. Miura, S., et al., *The mechanism of railway tracks.* Japan Railway & Transport Review, 1998. **3**: p. 38-45.

44. Sadri, M. and M. Steenbergen, *Effects of railway track design on the expected degradation: Parametric study on energy dissipation.* Journal of Sound and Vibration, 2018. **419**: p. 281-301.
45. Li, D. and E.T. Selig, *Method for Railroad Track Foundation Design. I: Development.* Journal of Geotechnical Engineering, 1998. **124**(4): p. 316-322.
46. Chrismer, S., *Test of Geoweb to improve track stability over soft subgrade*. 1997, Association of American Railroads: Washington DC.
47. Zhou, H. and X. Wen, *Model studies on geogrid-or geocell-reinforced sand cushion on soft soil.* Geotextiles and Geomembranes, 2008. **26**(3): p. 231-238.
48. Liu, Y., A. Deng, and M. Jaksa, *Three-dimensional modeling of geocell-reinforced straight and curved ballast embankments.* Computers and Geotechnics, 2018. **102**: p. 53-65.
49. Kaewunruen, S., et al., *Field performance to mitigate impact vibration at railway bridge ends using soft baseplates*, in *11th World Congress on Railway Research*. 2016: Milan, Italy.
50. Elliott, R.P. and S.I. Thornton, *Resilient modulus and AASHTO pavement design.* Transportation research record, 1988(1196).
51. Li, D. and E.T. Selig, *Resilient Modulus for Fine-Grained Subgrade Soils.* Journal of Geotechnical Engineering, 1994. **120**(6): p. 939-957.
52. Christopher, B.R., C. Schwartz, and R. Boudreau, *Geotechnical aspects of pavements* F.H. Administration, Editor. 2006: Washington, D.C.
53. Budhu, M., *Soil mechanics fundamentals*. 2015: John Wiley & Sons.
54. Lekarp, F., U. Isacsson, and A. Dawson, *State of the art. II: Permanent strain response of unbound aggregates.* Journal of transportation engineering, 2000. **126**(1): p. 76-83.
55. Thompson, M.R. and Q.L. Robnett, *Resilient properties of subgrade soils*. 1976.
56. Moossazadeh, J. and M.W. Witczak, *Prediction of subgrade moduli for soil that exhibits nonlinear behavior*. Transportation Research Record, 1981(810).
57. Brown, S., A. Lashine, and A. Hyde, *Repeated load triaxial testing of a silty clay.* Geotechnique, 1975. **25**(1): p. 95-114.
58. Fredlund, D., A. Bergan, and E. Sauer, *Deformation characterization of subgrade soils for highways and runways in northern environments.* Canadian Geotechnical Journal, 1975. **12**(2): p. 213-223.
59. Raymond, G., P. Gaskin, and F. Addo-Abedi, *Repeated compressive loading of Leda clay.* Canadian Geotechnical Journal, 1979. **16**(1): p. 1-10.
60. Drumm, E., Y. Boateng-Poku, and T. Johnson Pierce, *Estimation of subgrade resilient modulus from standard tests.* Journal of Geotechnical Engineering, 1990. **116**(5): p. 774-789.
61. Shackel, B. *The derivation of complex stress–strain relations*. in *Proc. 8th Int. Conf. on Soil Mech. and Found. Engrg*. 1973.
62. Uzan, J., *Characterization of granular material*. Transportation research record, 1985. **1022**(1): p. 52-59.
63. Mengelt, M., T.B. Edil, and C.H. Benson, *Resilient modulus and plastic deformation of soil confined in a geocell.* Geosynthetics International, 2006. **13**(5): p. 195-205.
64. R. Janaidhanam and C.S. Desai, *Three-dimensional testing and modeling of ballast.*

65. Edil, T.B. and P.J. Bosscher, *Engineering properties of tire chips and soil mixtures.* Geotechnical testing journal, 1994. **17**(4): p. 453-464.
66. Al-Qadi, I. and J. Hughes, *Field evaluation of geocell use in flexible pavements.* Transportation Research Record: Journal of the Transportation Research Board, 2000(1709): p. 26-35.
67. Pokharel, S.K., et al., *Behavior of geocell-reinforced granular bases under static and repeated loads*, in *Contemporary Topics in Ground Modification, Problem Soils, and Geo-Support*. 2009. p. 409-416.
68. Henkel, D. and G. Gilbert, *The effect measured of the rubber membrane on the triaxial compression strength of clay samples.* Geotechnique, 1952. **3**(1): p. 20-29.
69. Bolton, M., *The strength and dilatancy of sands.* Geotechnique, 1986. **36**(1): p. 65-78.
70. Bolton, M., *Discussion: The strength and dilatancy of sands.* Geotechnique, 1987. **37**(2): p. 219-226.
71. Li, D. and E.T. Selig, *Cumulative plastic deformation for fine-grained subgrade soils.* Journal of Geotechnical Engineering 1996. **122**(12): p. 1006-1013.
72. Thakur, J.K., et al., *Performance of geocell-reinforced recycled asphalt pavement (RAP) bases over weak subgrade under cyclic plate loading.* Geotextiles and Geomembranes, 2012. **35**: p. 14-24.
73. Australian Rail Track Corporation, *Track Reconditioning Guidelines*, in *Engineering Practices Manual - Civil Engineering*. 2006: NSW.
74. Kaewunruen, S., Sussman, J.M., Mutsumoto, A. Grand challenges in transportation and transit systems. *Front. Built Environ*. 2016, 2, 4